Charles University

Faculty of Science

Study programme: Physical Chemistry

Bc. Peter Illés

Study of morphology and degree of ionization of block copolymers

Studium morfologie a stupně ionizace blokových kopolymerů

Diploma thesis

Supervisor: **Ing. Lucie Nová, Ph.D.**

Consultant: **Mgr. Michal Mazur, Ph.D.**

Prague, 2025

Prohlašuji, že práci jsem sepsal samostatně, všechny použité zdroje a literatura jsou v práci řádně citovány a práce nebo její podstatná část nebyla využita jako závěrečná práce k získání jiného nebo stejného akademického titulu. V této práci byla uměla inteligence využita výhradně ke zlepšení čitelnosti textu a k opravám jazykových chyb.

Praha, 22. 8. 2025 Bc. Peter Illés

I would like to thank my supervisor Ing. Lucie Nová, Ph.D. for her guidance throughout the creation of this thesis. My gratitude also goes to prof. RNDr. Filip Uhlík, Ph.D. for his valuable insights and unending technical support. I would further like to thank the members of Soft Matter Theory Group for their support and collaboration.

Finally, I would like to express my heartfelt gratitude to my family for their support and patience throughout my studies. This thesis is dedicated to the memory of my grandmother, who sadly passed away just a few weeks before its completion. Her love and support remain an enduring source of strength.

Abstract

Block copolymers are an important class of macromolecular materials, due to their high tunability. In this work we studied two types of copolymers, doubly hydrophilic and amphiphilic block copolymers. Our study was conducted through simulations, using Hamiltonian Monte Carlo with a coarse-grained copolymer model. We observed the effects of chain length, ionization, and concentration on the overall behaviour of the polymer system. For the doubly hydrophilic copolymers, we found a mixture of size scaling behaviours consistent with those reported in the scientific literature. In the case of amphiphilic copolymers, we observed clear aggregation trends.

Keywords

molecular simulations, self-assembly, responsive systems, block copolymers, weak polyelectrolytes, strong polyelectrolytes

Abstrakt

Blokové kopolymery jsou důležitým typem makromolekulárních materiálů, kvůli jednoduché laditelnosti jejich vlastností. V této práci jsme se věnovali dvěma typům blokových kopolymerů, a to dvojnásobně hydrofilním a amfifilním. Tyto systémy byly studovány pomocí výpočetní metody hamiltonovské Monte Carla za použití zhrubeného modelu kopolymeru. Důraz byl kladen na vlivy délky řetězců, ionizace a koncentrace na celkové chování polymerních systémů.U dvojnásobně hydrofilních kopolymerů bylo pozorováno škálování velikosti rětězců, které je v souladu s dosavadní vědeckou literaturou. V systémech amfifilních kopolymerů byla pozorována zřetelná agregace.

Klíčová slova

molekulové simulace, samoskladba, responzivní systémy, blokové kopolymery, slabé polyelektrolyty, silné polyelektrolyty

List of Abbreviations

DNA - deoxyribonucleic acid

RNA - ribonucleic acid

PE - polyethylene

PP - polypropylene

PVC - polyvinyl chloride

PS - polystyrene

SANS - small-angle neutron scattering

MANIAC - mathematical analyzer, numerical integrator, and computer

SRS - soft repulsive sphere

SAS - soft attractive sphere

MD - molecular dynamics

EOM - equations of motion

MC - Monte Carlo

MCMC - Markov chain Monte Carlo

FFT - fast Fourier transform

ScaFaCoS - scalable fast Coulomb solvers

PBC - periodic boundary conditions

Contents

1 Introduction **8**

1.1 Polyelectrolytes 9

1.2 Block Copolymers 10

1.3 Solvent Quality 11

1.4 Concentration of Polymer Solutions 12

1.5 Studied System 15

2 Methods **16**

2.1 Chain Model 18

2.1.1 Coarse Grained Approach 19

2.1.2 Potentials 21

2.1.3 Different Bead Representations 25

2.2 Simulation Method 27

2.2.1 Monte Carlo 27

2.2.2 Molecular Dynamics 30

2.2.3 Hamiltonian Monte Carlo 32

2.3 Technical Details 32

2.4 Simulation Protocol 34

3 Results and Analysis **37**

3.1 Doubly Hydrophilic Copolymers 37

3.1.1 Effects of Chain Length 38

3.1.2 Effects of Ionization 42

3.1.3 Effects of Concentration 45

3.2 Amphiphilic Copolymers 48

3.2.1 Effects of Chain Length 48

3.2.2 Effects of Ionization 50

3.2.3 Effects of Concentration 50

4 Future perspectives **53**

5 Conclusion **55**

References **56**

Attachments **1**

1 Introduction

Polymers are an essential class of macromolecular materials, composed of covalently bonded repeating monomeric units. The defining feature, which distinguishes them from other macromolecules, is a chain-like architecture made out of long sequences of repeating units that may be linear, branched, or cross-linked. Polymers may be of either synthetic or natural origin[1].

Natural polymers include biomacromolecules such as DNA, RNA, proteins, and polysaccharides, which are fundamental to life. They provide structural support, store energy, transfer genetic information, and catalyze biochemical reactions. Historically, humans have relied on natural polymers such as cellulose, silk, wool, and natural rubber for material development. Modifying and processing these polymers led to important semi-synthetic substances, including vulcanized rubber, nitrocellulose, and celluloid, which laid the foundation for modern materials science and inspired the development of fully synthetic polymers[2].

Synthetic polymers are produced from monomers through controlled polymerization processes, most often using petrochemical feedstocks. The low cost, together with the ability to tune chemical structure, molecular weight, and morphology, has made synthetic polymers indispensable in modern society, although their widespread use has come at significant environmental cost. Examples include polyethylene (PE) and polypropylene (PP), which dominate packaging due to their low cost and versatility; polyvinyl chloride (PVC), widely used in construction; polystyrene (PS), employed in insulation; and polyesters and polyamides, which revolutionized textiles[3].

The overall architecture of the chain and the chemistry of the monomers dictate the material's physical and chemical properties. This versatility enables the rational design of polymers for a wide range of applications.

In this work, we focus on concentrated polymer solutions. Specifically, we investigate polyelectrolytes (Section 1.1), with particular emphasis on block copolymers (Section 1.2). We then examine the role of solvent quality (Section 1.3) and concentration effects (Section 1.4). Finally, in Section 1.5, we describe the model systems studied in this thesis.

1.1 Polyelectrolytes

Polyelectrolytes are polymers containing repeating units that undergo partial or full dissociation. Depending on the nature of their ionizable groups, they are classified as polyacids (negatively charged upon ionization) or polybases (positively charged). They are further categorized as strong or weak, depending on the extent of ionization.

Strong polyelectrolytes are almost fully ionized at equilibrium in aqueous solution. They possess functional groups that dissociate or associate into stable ions. For example, in neutral solution, strong polyacids dissociate to form stable anions, whereas strong polybases stabilize upon protonation. Once ionized, the charges can be treated as effectively static.

Weak polyelectrolytes, by contrast, are only partially ionized under equilibrium conditions, because their dissociated or associated ions are less stable. Their ionization is reversible, allowing charges to migrate along the chain via repeated cycles of dissociation and association. This enhances charge mobility and influences chain conformation and responsiveness to environmental changes, factors that will become important in our modeling.

Polyelectrolytes exhibit unique solution behavior due to chain charging. Electrostatic repulsion between charged segments drives the chains into more extended conformations. The addition of salt ions screens these repulsions, enabling the chains to adopt more compact conformations[4]. These behaviors are strongly influenced by polymer concentration (Section 1.4). The interplay between intrachain repulsion, interchain interactions, and salt-mediated screening can lead to stretching, collapse, aggregation, phase separation, or the formation of ordered structures. Such responsiveness makes polyelectrolytes excellent candidates for designing smart materials.

Tunable charge-related properties have attracted wide research interest across different disciplines. Applications include water purification and desalination[5], drug delivery systems[6], tissue engineering scaffolds[7], and responsive smart materials[8].

However, a fully ionizable chain is not always desirable. High charge densities can generate strong repulsions that restrict chain flexibility, in some cases reduce solubility, and compromise desired physical properties. One strategy to overcome these limitations

is the use of block copolymers, which combine charged and neutral segments within a single macromolecule. This architecture incorporates polyelectrolyte functionality where needed, while neutral blocks moderate charge density and improve solubility.

1.2 Block Copolymers

Copolymers consist of two or more distinct monomers. The arrangement of these monomers defines the polymer's architecture and properties (Figure 14).

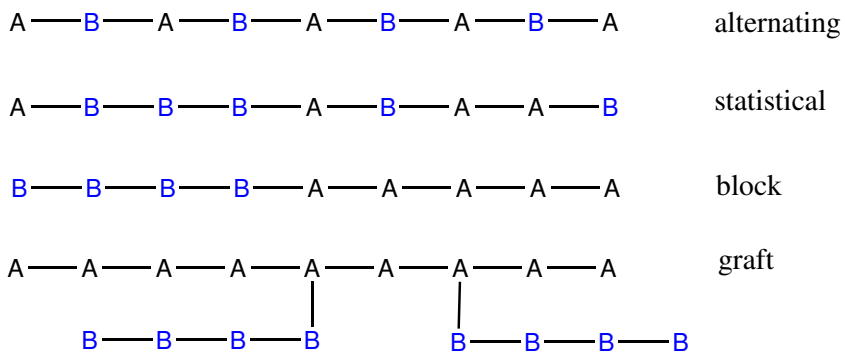

Figure 1: Different possible structures of copolymers.

A key subclass is the **block copolymer**, in which a chain is divided into distinct segments (blocks), each composed of a single type of monomer. Because each block retains its own chemical and physical characteristics, block copolymers are versatile materials that can be engineered for specific applications.

Due to the inherent differences between blocks, block copolymers often undergo microphase separation, forming well-defined morphologies such as spheres, cylinders, vesicles, and lamellae[9,10]. Solubility is particularly important in determining behavior, leading to two broad classes of interest here: amphiphilic block copolymers and doubly hydrophilic block copolymers.

Doubly hydrophilic block copolymers are especially versatile. One block promotes solubility in water, while the other may be stimuli-responsive or tailored for specific interactions. Some systems employ blocks that switch from hydrophilic to hydrophobic under external stimuli[11]. This flexibility enables a wide variety of supramolecular structures and functions. Reported applications include drug delivery[12,13], inorganic templating[14], nanoparticle growth control[15], sensing platforms[16], catalyst supports[17], and membrane fabrication for purification and separation[18].

Amphiphilic block copolymers have been studied extensively in materials science and biomedicine. Their hydrophilic–hydrophobic mismatch drives self-assembly into nanostructures such as micelles and vesicles[19]. This process is tunable via block length, solvent quality, concentration, temperature, and pH. These assemblies are highly useful in drug delivery: hydrophobic drugs can be encapsulated in the micellar core, while the hydrophilic corona provides stability, controlled release, and targeting capabilities[20]. Amphiphilic block copolymers also serve as nanoreactors, templates for material synthesis[21], and emulsifiers in industrial formulations[22].

The tunable self-assembly of block copolymers, combined with their chemical versatility, makes them indispensable for designing next-generation functional materials.

1.3 Solvent Quality

Solvent quality, a central concept in polymer science, describes how polymer chains interact with their surrounding solvent. These interactions govern polymer conformation, solubility, and ultimately the physical properties of polymer solutions. Solvent quality is typically classified as *good*, *theta* (θ), or *poor*:

- **Good solvent:** polymer segments prefer interacting with solvent molecules rather than with each other.
- **Theta solvent (θ):** polymer–polymer and polymer–solvent interactions are balanced; chains behave as ideal random coils.
- **Poor solvent:** polymer segments prefer interacting with each other, leading to collapse or precipitation.

The Flory–Huggins theory quantifies solvent quality via the interaction parameter χ:

$$\chi = \frac{z}{k_B T}\left(\varepsilon_{12} - \frac{\varepsilon_{11} + \varepsilon_{22}}{2}\right), \tag{1}$$

where z is the coordination number (the number of nearest neighbors on the lattice), k_B is the Boltzmann constant, and T is the absolute temperature. The parameters ε_{12}, ε_{11}, and ε_{22} denote the pairwise interaction energies between polymer–solvent, polymer–

polymer, and solvent–solvent contacts, respectively.

Parameter $\chi < 0.5$ indicates a good solvent, $\chi = 0.5$ corresponds to a theta solvent, and $\chi > 0.5$ corresponds to a poor solvent.

The radius of gyration R_g reflects solvent quality:

$$R_g \propto N^{\nu}, \tag{2}$$

with $\nu \approx 0.6$ in good solvents, $\nu = 0.5$ in theta solvents, and polymers collapsing in poor solvents. These conformational changes influence viscosity, diffusion, and phase behavior[23]. Techniques such as light scattering, small-angle neutron scattering (SANS), and viscometry provide experimental access to these effects[24].

1.4 Concentration of Polymer Solutions

The concentration of polymer systems plays a crucial role in determining their structural and dynamical properties. As the concentration of polymer chains increases, intermolecular interactions become increasingly significant, leading to deviations from ideal chain behavior observed in dilute solutions[24]. In particular, the scaling of polymer size, such as the radius of gyration, with respect to density reflects transitions from dilute to semidilute and concentrated regimes, where excluded volume effects and chain entanglements dominate[23].

In the simplest case of a homopolymer in a dilute solution and good solvent, the dominant interactions are intrachain rather than interchain. In this regime, the distance between polymer chains is sufficiently large that interchain interactions are negligible. These chains form isolated coils.

As polymer concentration increases, the distance between chains decreases. Eventually, the spacing between coils becomes comparable to their size. This critical concentration is known as the overlap concentration, c^*, defined as the concentration at which volumes of individual coils begin to overlap and interpenetrate.

Beyond c^*, polymer coils no longer remain isolated and instead form a semi-dilute

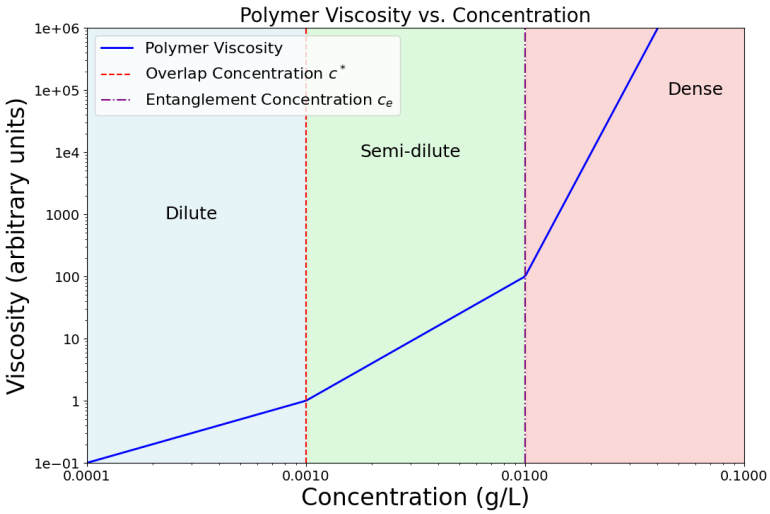

Figure 2: Dependence of viscosity on concentration of polymer solution. Redrawn from Polymer Physics by Rubinstein et al.[23].

network of overlapping coils. At higher concentrations above c^*, chains may eventually become entangled, leading to dramatic changes in rheological and dynamical properties. An example of this scaling is shown in Figure 2.

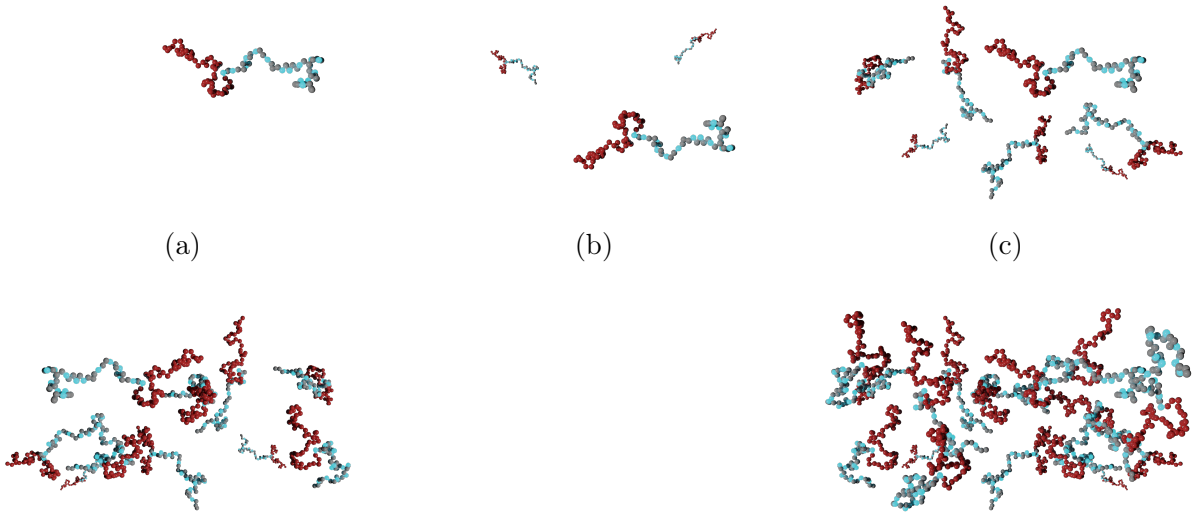

Figure 3: Visual representation of polymer chains in different regimes. (a) Dilute regime — essentially no interaction; (b) Dilute regime at higher concentration — negligible interactions; (c) Approaching overlap concentration — coil sizes comparable to interchain distances; (d) Beyond overlap concentration — significant chain interactions; (e) Entanglement concentration — concentrated regime, chains are entangled.

Polyelectrolyte solutions present a more complex scenario due to the charged polymer

chains interacting both within themselves and with other chains. At low concentrations, electrostatic repulsions cause the chains to stretch into extended conformations. However, long-range Coulomb interactions are mitigated by counter-ions and solvent molecules, which screen the charges.

The system's behavior is strongly influenced by polymer concentration, especially in relation to the interaction and overlap concentrations. The *interaction concentration*[25] is reached when the screening length becomes comparable to the average distance between chains, forcing direct interactions between charges. In contrast, the *overlap concentration* marks the threshold at which coil dimensions match interchain spacing. Typically, the interaction concentration occurs before the overlap concentration.

Beyond the overlap concentration, the properties and scaling behavior of the system change significantly. At even higher concentrations, the solution approaches the entanglement concentration, where chains become physically entangled and, from an electrostatic perspective, contribute substantially to charge screening. Such systems are highly sensitive to the electrostatic environment.

1.5 Studied System

In recent decades, extensive theoretical, computational, and experimental work has been devoted to understanding the scaling behavior of polymer and polyelectrolyte solutions. Building upon these studies, we aim to extend the understanding of scaling laws by considering block copolymer systems that combine distinct classes of monomeric interactions. In particular, we focus on block copolymers comprising one polyelectrolyte block and a second block that is either hydrophilic or hydrophobic. The inherent contrast between these blocks is expected to generate a rich interplay of conformational behaviors and scaling regimes, thereby producing a combination of effects not accessible in homopolymer systems. Furthermore, we investigate how external parameters, such as polymer concentration and degree of ionization, modulate these behaviors.

As a primary structural measure, we employ the radius of gyration, defined as

$$R_g = \sqrt{\frac{1}{N}\sum_{i=1}^{N} |\mathbf{r}_i - \mathbf{r}_{\mathrm{cm}}|^2}, \tag{3}$$

where N denotes the number of monomers, $\mathbf{r}i$ the position of the ith monomer, and $\mathbf{r}$cm the chain's center of mass. The radius of gyration provides a fundamental and broadly applicable measure of the overall size of macromolecular objects, independent of their specific shape[26].

2 Methods

Theoretical methods have become an integral tool for studying chemical systems, ranging from simple molecules to large, complex assemblies. Since their development in the late 1940s and 1950s, these methods have consistently proven valuable for investigating material properties at the microscopic level. One of the first groundbreaking studies in this field was done by Metropolis *et al.*[27]. Their study consisted of a simulation of a system with the maximum of 224 particles in 2D space, modeled as rigid discs. This simulation was performed over 48-–64 cycles on MANIAC (Mathematical Analyzer, Numerical Integrator, and Computer), an early pioneering computer. Under this setup, obtaining a single point on the pressure curve required approximately 4–5 hours. Although they were

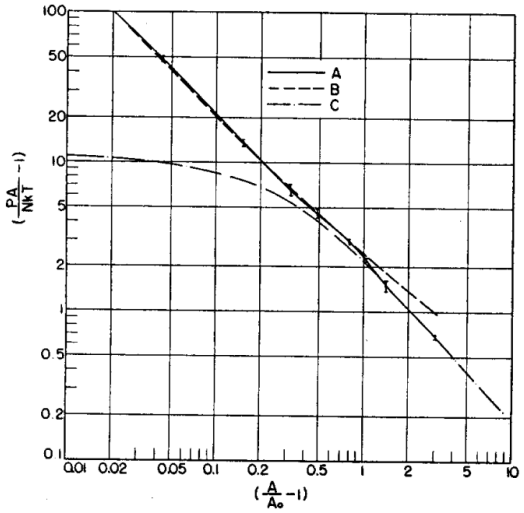

Figure 4: Pressure curve from Metropolis behaviour[27]. Pressure (y-axis) vs. reduced density (x-axis, log–log scale). Solid line: computational results; dashed/dash-dotted lines: theoretical predictions.

unable to observe any phase transition behaviour (later understood as an inherent limitation of the rigid-sphere approximation) successfully predicted system pressure within a few percent of theoretical values. This demonstrated the potential of computer simulations as a reliable tool for studying condensed matter systems. The work of Metropolis *et al.* will be revisited in Section 2.2 when discussing the ingenious algorithm that allowed these computations. With the rapid increase in computational power, such simulations have become significantly less costly, and the same calculations can now be completed within seconds. MANIAC could perform about 10,000 operations per second[28], whereas today's fastest supercomputers like Frontier perform over 10^{18} operations per second[29],

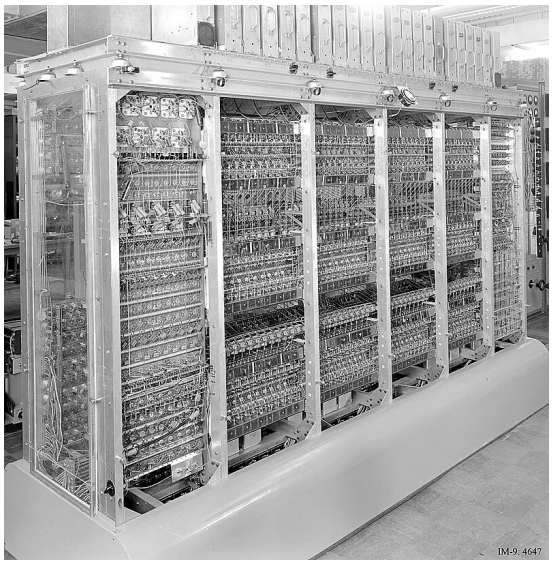

(a) MANIAC (1952) – 10,000 operations/sec

(b) Frontier (2023) – $>10^{18}$ operations/sec

Figure 5: Comparison of computing power: MANIAC vs. Frontier Supercomputer

making them approximately 10^{14} times faster. This enables the study of significantly larger or more detailed systems.

Two main branches of theoretical chemical computations can be distinguished:

Quantum Mechanical Methods, although not relevant for this study, are a very important class of methods which rely on quantum mechanics as a basis for calculations. They attempt to describe the electronic structure of materials or molecules and from that model their fundamental properties. The main limitation of these methods lies in the rapidly increasing computational complexity. The size of the system which is calculated is very limited and therefore are not very well suited for systems with many species. These methods can be further categorized by the type of approximations employed. Notable examples include semi-empirical methods, which employ parametrization of some computationally expensive quantum-mechanical equations. Another important category are *ab initio* methods, which attempt to solve electronic Schrödinger equation, using approximations building from the ground up. Lastly, there are also density functional methods, which deal with electronic density rather than behaviour of singular electrons. This leads to good precision for a fraction of the computation time.

Empirical Methods are methods based on using empirical force fields to describe interactions between atoms. These methods neglect quantum effects entirely. Instead, they rely on classical physics to compute energies and forces, using parameterized functions

for bonds, angles, torsions, and non-bonded interactions. Their main advantage lies in computational efficiency, allowing simulation of very large systems. However, this comes at the cost of limited detail and accuracy, especially when modeling chemical reactions or unusual environments. Empirical methods are best suited for systems where high-level quantum accuracy is not essential, and where the goal is to model structural, thermodynamic, or dynamic behaviour at large scale.

An important factor to consider for any simulation is the complexity of the simulated environment and chemical species. Even the most powerful methods in terms of speed slowly approach a territory in which their effectivity slowly deteriorates. A well-designed simulation requires a computer model that captures the essential features of the system. In the case of polymers, this means developing a representation of the polymer chain that balances chemical and physical accuracy with computational efficiency.

2.1 Chain Model

As stated before, one of the most important things to consider when designing a simulation is the modeling of the chemical species present. The objective is to capture the key structural and energetic features of the molecule we aim to study, while still maintaining a decent computational time. Often this proves difficult. As an example, consider the system under investigation, that is a concentrated system of polymer chains. Some approaches, particularly quantum mechanical methods, scale exponentially with system size. While this approach provides exceptionally precise data and is well-suited for small atomic clusters, it becomes computationally infeasible for larger systems. Therefore we must instead employ empirical methods and represent interactions of our atoms as parametrized empirical functions. This approach substantially reduces computational cost, although some accuracy is sacrificed. Even with this simplification, the resulting simulations may remain computationally infeasible. For instance, a simple monomer of polyacrylic acid can be considered.

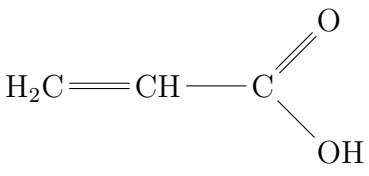

To model this simple molecule, we have to account for 8 bonding potentials, 9 angular potentials and 9 non-bonding potentials in a very simple interaction model. If we were to do this for a 10 000 of such monomers, it would no longer be feasible. In practice we use models which heavily vary in the degree of detail. The following section discusses one such approach.

2.1.1 Coarse Grained Approach

We have previously mentioned that modeling chemical species requires adaptations based on complexity and what characteristics one wishes to observe. In general three main categories of models are commonly distinguished for representing chemical species.

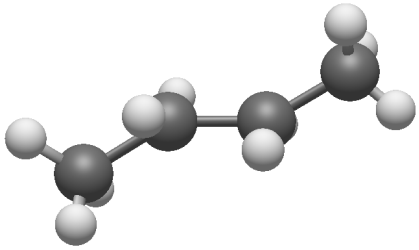

(a) All-atom butane molecule

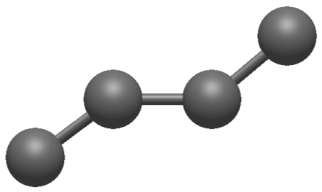

(b) United-atom butane molecule

(c) Coarse grained butane molecule

Figure 6: Comparison of different representations of butane molecule.

All-atom models which replicate the chemistry of the given species as closely as possible. Each of the atoms has their own properties like mass, charge, van der Waals radius and all of its potentials. Aim of these models is to closely mimic the behaviour of the atom. These models are particularly suited for observing specific detailed interactions

between active chemical groups and microstructural properties.

United-atom models simplify molecular representations by combining hydrogen atoms with the heavier atoms to which they are bonded. Each resulting united atom retains properties of the group, such as mass, charge, and interaction potential. This helps significantly reduce the number of interactions that need to be computed. These models are well-suited for larger systems or longer timescales, where full atomic detail is unnecessary, but retaining chemical specificity and structural accuracy remains important.

Coarse-grained models represent groups of atoms as single interaction sites or "beads", ignoring most of the atomic detail. Each bead comprises of collective properties of multiple atoms it represents, such as size, mass, and effective interactions. These models are ideal for simulating very large systems or long timescales where atomic resolution is unnecessary. Coarse-grained models allow better exploration of global structure, dynamics, and self-assembly, while sacrificing some detailed chemical information.

This study focuses on coarse-grained model of block copolymer chain. This approach yields a considerable decrease in computational time, whilst still retaining a satisfactory level of detail in our observables. Since the main point of our interest is morphology and assembly of our polymer chains, This level of detail is expected to provide sufficient information about the formed structures. We base this assumption from many scientific works, which have been done using these model with respectable results.[30,31]

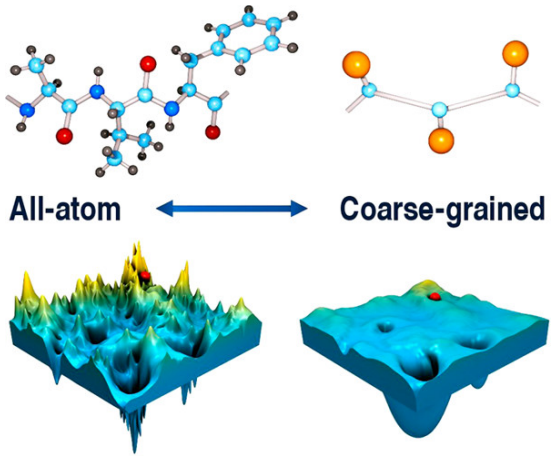

(a) Potential energy surface comparison of all-atom and coarse-grained model of protein[31]

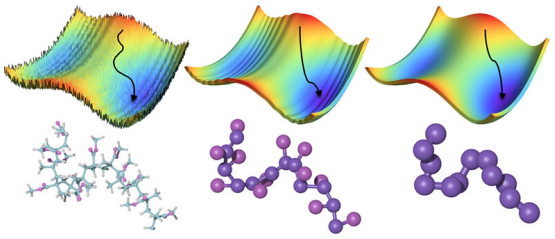

(b) Potential energy surface comparison of all-atom, united-atom and coarse-grained model of polymer[30]

Figure 7: Effects of coarse-graining on (a) protein molecules (b) polymer molecules potential energy surface.

Coarse-graining enables us to efficiently simulate high number of polymer chains and explore their self-assembly and morphological properties. We will approximate our monomers as single beads with properties dependent on monomer being represented. In each system there will be maximum of three types of polymer beads and a single type of counter-ion bead. Interactions between beads will be realized by potentials, which will be discussed in the next section.

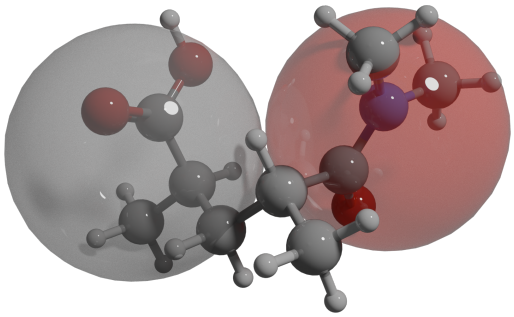

Figure 8: Visual representation of our coarse-grained polymer beads.

2.1.2 Potentials

Our coarse grain beads will be placed in an implicit solvent, which has no structure and is characterized by relative permittivity of water. Bonded interactions are represented by a harmonic potential

$$U_{\mathrm{b}} = \varepsilon_{\mathrm{b}} \left(\frac{r}{r_0} - 1 \right)^2 , \tag{4}$$

where $\varepsilon_b = 80.0\, k_B T$ is the spring constant describing the stiffness of the massless bond, r is the instantaneous separation between the two bonded beads, and $r_0 = 0.3\,\mathrm{nm}$ is the equilibrium bond length corresponding to the minimum of U_b. Harmonic potential is one of the most widely used models for describing bonded interactions in coarse-grained simulations, particularly for larger molecules such as polymers and biomacromolecules.[32,33] It assumes that the bond behaves like an ideal spring, with the restoring force proportional to the displacement from the equilibrium bond length.

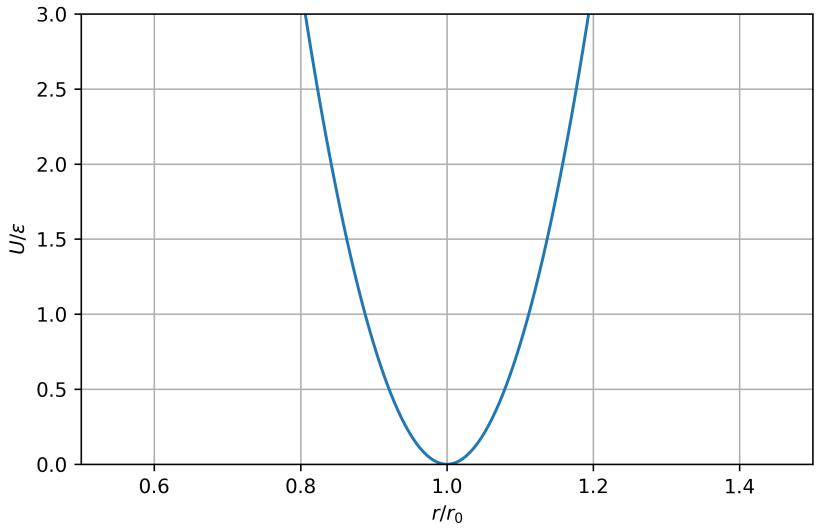

Figure 9: Harmonic bonding potential with minimum value at $r = r_0$

To represent interaction between two non-bonded beads we will add non-bonding potentials. There will be two types of these potentials, depending on the bead that's being represented. First and the most basic case will be modeled by soft sphere repulsion (SRS) potential. Mathematically this potential can be written as

$$U_{\text{srs}} = \varepsilon_{\text{nb}} \left(\frac{r - c}{r} \right)^2, \tag{5}$$

where $\varepsilon_{\text{nb}} = 1\, k_{\text{B}}T$, r is the instantaneous distance between two beads and $c = 2r_0$ is cut-off distance at which $U_{\text{srs}} = 0$. This will be used as a basis for all beads. The soft sphere repulsion potential represents a purely repulsive, short-range interaction between two non-bonded beads. Its role is to prevent beads from overlapping by penalizing configurations where they come closer than a prescribed cutoff distance. Unlike hard-sphere models, where overlap is strictly forbidden, the SRS allows a smooth and continuous rise in energy as the distance decreases, which makes it more suitable for molecular simulations.

Beads representing hydrophobic monomers are assigned an additional non-bonded interaction in the form of soft attractive sphere potential (SAS). Mathematically in form of

$$U_{\text{sas}} = -\varepsilon_{\text{nb}} \frac{27r}{4c} \left(\frac{r}{c} - 1 \right)^2, \tag{6}$$

where like-wise $\varepsilon_{\text{nb}} = 1\, k_{\text{B}}T$, r is the distance between two beads and $c = 2r_0$ is cut-off

distance at which $U_{\text{srs}} = 0$. This introduces an energetic preference for hydrophobic beads to remain in close proximity, mimicking the effective attraction caused by the hydrophobic effect in coarse-grained models. Both SRS and SAS can be seen in Figure 10, along

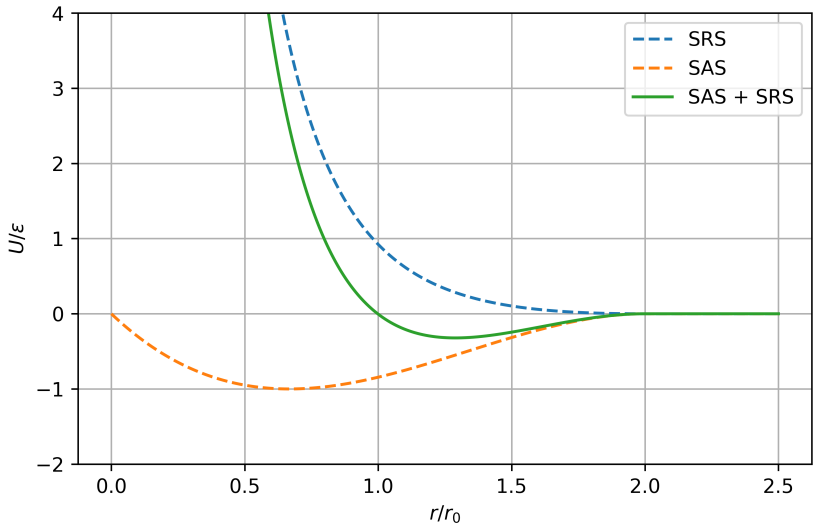

Figure 10: Soft repulsive sphere (SRS) and soft attractive sphere (SAS) potentials, along with the resulting combined potential applied to hydrophobic beads.

with the resulting potential, which will subsequently be applied to hydrophobic beads. Furthermore, we introduce a parameter θ to modulate the strength of the attractive potential. The resulting potential is expressed as

$$U_{\text{nb}} = U_{\text{srs}} + U_{\text{sas}} \cdot \theta, \tag{7}$$

providing a convenient means of tuning the hydrophobic interaction. The resulting potentials for various θ values are shown in Figure 11.

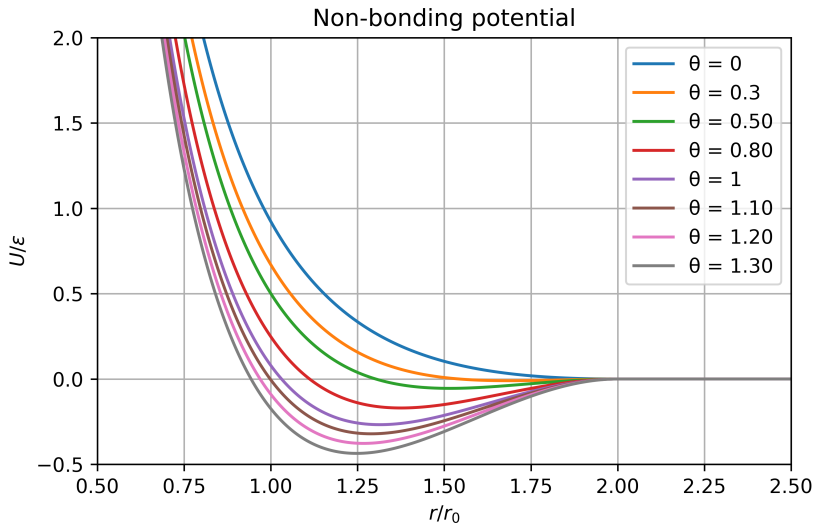

Figure 11: Non-bonding potentials for hydrophobic beads at different θ parameter values.

To explore the influence of this parameter, we performed simulations of multiple polymer chain lengths at different θ values, measuring the end-to-end distance R_e. It is well established that in a θ-solvent, a polymer chain behaves ideally, and its end-to-end distance scales proportionally with the number of monomers.[34,35] The results of this study are presented in Figure 12. From these results, we deduce that the θ value corresponding to θ-solvent conditions is approximately 1.0.

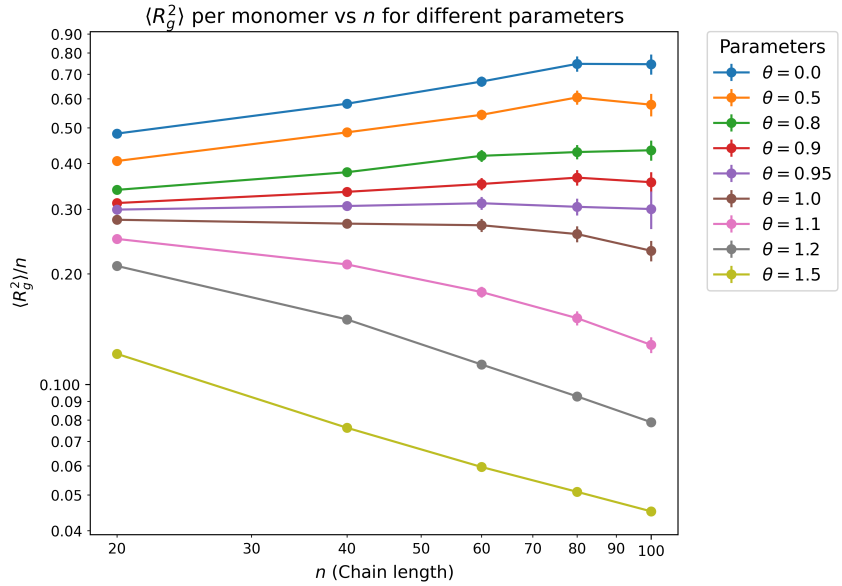

Figure 12: End-to-end distances of polymer chains as a function of chain length for different θ values.

Finally, the electrostatic interactions between charged beads are described using the Coulomb potential expressed in terms of the Bjerrum length l_B:

$$U_{\text{coul}} = k_B T \frac{Z_1 Z_2}{r/l_B}, \tag{8}$$

where r is the separation of the two charges, Z_1 and Z_2 are the corresponding valencies, k_B is the Boltzmann constant, and T is the temperature. The Bjerrum length l_B is defined as the separation at which the electrostatic interaction between two elementary charges equals the thermal energy $k_B T$, and is given by[36] $l_B = e^2/(4\pi\varepsilon_0\varepsilon_r k_B T)$. In our simulations, l_B is set to 0.7 nm to reflect the screening properties of water[37]. The form of this potential is illustrated in Figure 13, illustrating its characteristic $1/r$ decay.

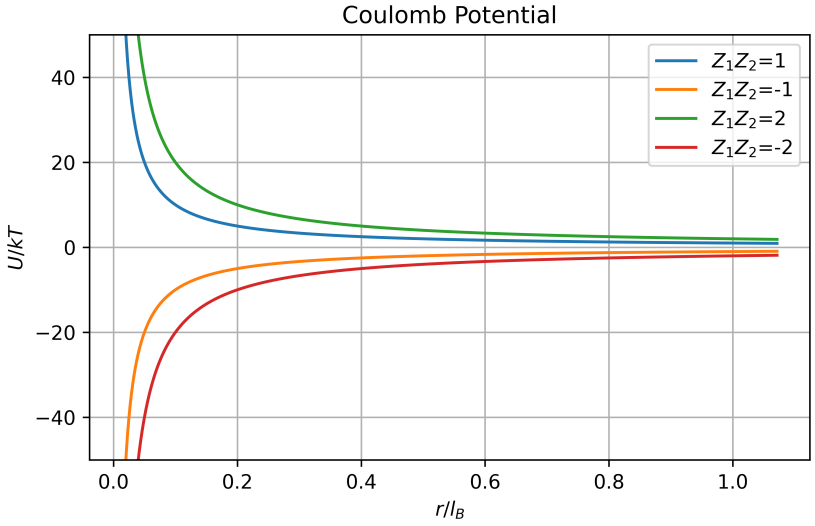

Figure 13: Coulomb potential between charged beads expressed in terms of the Bjerrum length l_B. Different products of Z_1 and Z_2 in different colours.

2.1.3 Different Bead Representations

Now that we have discussed the different interaction potentials acting on our beads, we summarize the bead representations employed in our simulations. As stated previously, each bead corresponds to either a single monomer or a counter-ion. For simplicity, all bead types are assigned the same nominal mass. Since our study focuses on equilibrium conformational properties rather than dynamical behaviour, the precise value of the bead mass does not play a significant role.

Polymer bead is approximated as a sphere with bonding and non-bonding potentials.

There will be two possible versions of this bead depending on the system under investigation:

- Hydrophilic - These beads interact only via repulsive forces in addition to the bonded potential.
- Hydrophobic - In this case, beads exhibit a combination of attractive and repulsive non-bonded interactions with other hydrophobic beads, while maintaining purely repulsive interactions with beads of different character.

Polyelectrolyte bead is represented as a bead which is capable of acquiring a charge. In our simulation, we will consider only monovalent polyanions, therefore the acquired charge on the chain will always be negative. When bead is ionized a positive counter-ion is inserted into simulation box and charge is given to the ionized polyelectrolyte bead. Charged beads will have Coulomb, bonding and hydrophilic non-bonding potentials acting on them. Note that our simulations only considered partial degrees of ionization, therefore all polyelectrolyte beads, which remain uncharged will behave as hydrophilic polymer beads. Furthermore we will have two types of ionizations:

- Strong - The negative charge on each monomer is static, meaning it does not change during the simulation.
- Weak - The negative charge on monomers is dynamic, allowing charge hopping between monomers. Charge hopping can be represented by the following chemical equilibrium:

  $$\mathrm{X^- + H^+ + YH \rightleftharpoons XH + Y^- + H^+}$$

  Here, the negative charge moves from monomer X to different monomer Y, maintaining the total charge of the chain but redistributing it dynamically.

Counter-ion bead is similar in nature to charged polyelectrolyte bead, with coulombic and non-bonding potential. These beads are non-bonded and therefore lack bonded interactions.

Figure 14: Color scheme used for beads in this work. From left to right: grey – polymer bead, red – uncharged polyelectrolyte bead, blue – charged polyelectrolyte bead, and green – counter-ion bead.

2.2 Simulation Method

In statistical mechanics, the properties of a system at equilibrium are determined by averaging over all possible microscopic states, weighted according to their statistical probability. This procedure is formally expressed through the partition function, which involves an integration over the system's entire phase space. However, the dimensionality of phase space grows rapidly with the number of particles, making direct evaluation practically impossible for all but the simplest systems.

Molecular simulations provide a way to overcome this challenge by generating representative samples of the phase space. These sampled configurations can then be used to compute ensemble averages of system properties.

Two of the most widely used approaches are Molecular Dynamics (MD) and Monte Carlo (MC) simulations[38].

2.2.1 Monte Carlo

Monte Carlo is a method often used in non-deterministic problems. Fundamentally, the Monte Carlo (MC) method is simply the use of random numbers to estimate mathematical quantities. The idea is to generate a large number of random values and use statistical averaging to approximate integrals or probabilities that would be difficult to evaluate analytically.

To illustrate the principle, two simple examples are considered: estimating the area of a circle and simulating dice rolls. π can be estimated by randomly placing points inside a unit square and counting the fraction that falls within a unit circle.

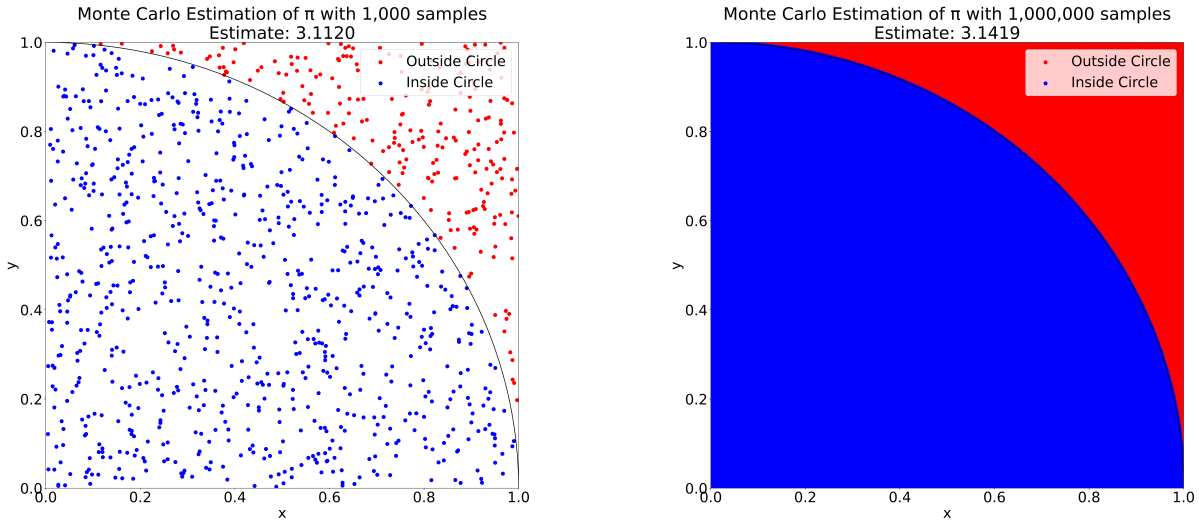

(a) (b)

Figure 15: Estimating π by sampling random points inside a square and checking if they fall within a circle. (a) 1 thousand cycles (b) 1 million cycles

Analogously, when rolling two dice and recording the sum of their faces, one can count the frequency of each possible outcome and normalize these frequencies to obtain the corresponding discrete triangular distribution. This distribution is symmetric and centered around the expected value of 7.

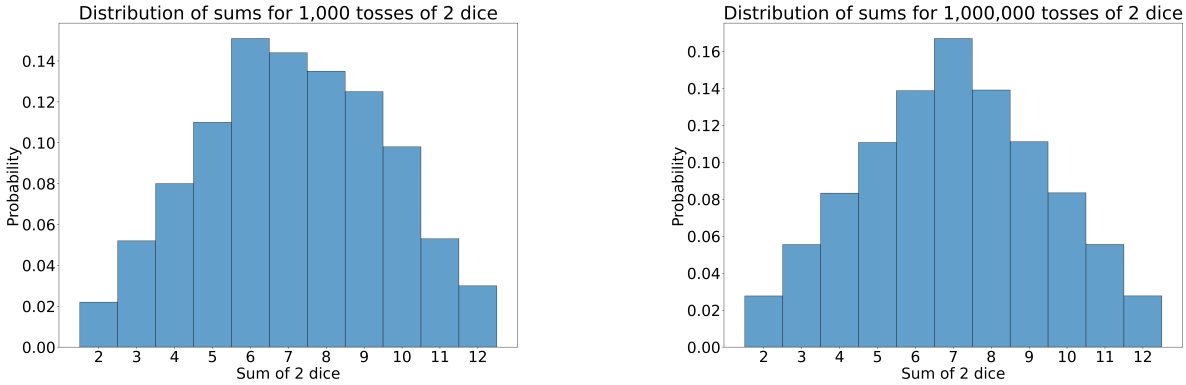

(a) (b)

Figure 16: Estimating a distribution of sum of dice rolls with two dice. (a) 1 thousand cycles (b) 1 million cycles

These results demonstrate that even with purely random numbers, certain inherent properties of systems can be reproduced. Although the probability distribution of two dice

rolls can be derived analytically in a straightforward manner, this example is presented here as a very straightforward demonstration of the Monte Carlo approach. While this simple Monte Carlo approach is effective for illustrative tasks, such as estimating π or simulating dice rolls, it quickly becomes impractical for molecular simulations.

Consider a system of chemical species with potential energy U_{pot}, defined as a function of the particle coordinates r_i. If random coordinates were generated uniformly, as in the earlier illustrative examples, most configurations would correspond to extremely high (or, less frequently, very low) energies. Consequently, ensemble averages of observables computed over such uniformly sampled states would lack physical meaning, since in reality different states occur with different probabilities.

An analogy with dice rolls further clarifies this point. If, instead of simulating the physical process of rolling two dice, one were to generate random integers uniformly between 2 and 12, the resulting probabilities would form a flat distribution. In this artificial case, the expected value would deviate from the correct value of 7, because in the real dice experiment the sums from 2 to 12 follow a discrete triangular distribution rather than being equally likely.

Importance sampling presents a solution for this problem. Rather than drawing states uniformly from all possibilities, importance sampling generates random samples according to a probability distribution that reflects the system's properties. In the dice example, this would correspond to drawing outcomes from the empirical probability distribution shown in Figure 16. In Monte Carlo molecular simulations, the Metropolis–Hastings algorithm is employed.

The Metropolis-Hastings algorithm is a Markov Chain Monte Carlo (MCMC) method that generates a sequence of configurations distributed according to the Boltzmann distribution. Originally programmed by Arianna W. Rosenbluth and first introduced in already mentioned article by Metropolis et. al[27]. Starting from an initial configuration, a trial move is proposed (for example, displacing a particle or rotating a molecule). The change in potential energy, $\Delta U = U_{\text{new}} - U_{\text{old}}$, is then evaluated. The trial move is accepted with probability

$$P_{\text{accept}} = \min\left(1, e^{-\beta \Delta U}\right), \tag{9}$$

where $\beta = 1/(k_B T)$.

If the move is accepted, the new configuration is saved. If not, the system remains in its current state. Most proposed moves that correspond to very high-energy configurations are automatically rejected, while energetically favorable or somewhat unfavorable moves are accepted according to their statistical weight. Repeating this over many cycles samples the Boltzmann distribution. This ensures that ensemble averages calculated from the simulation correspond to physically meaningful thermodynamic quantities. Metropolis Monte Carlo also by definition samples in canonical (NVT) ensemble.

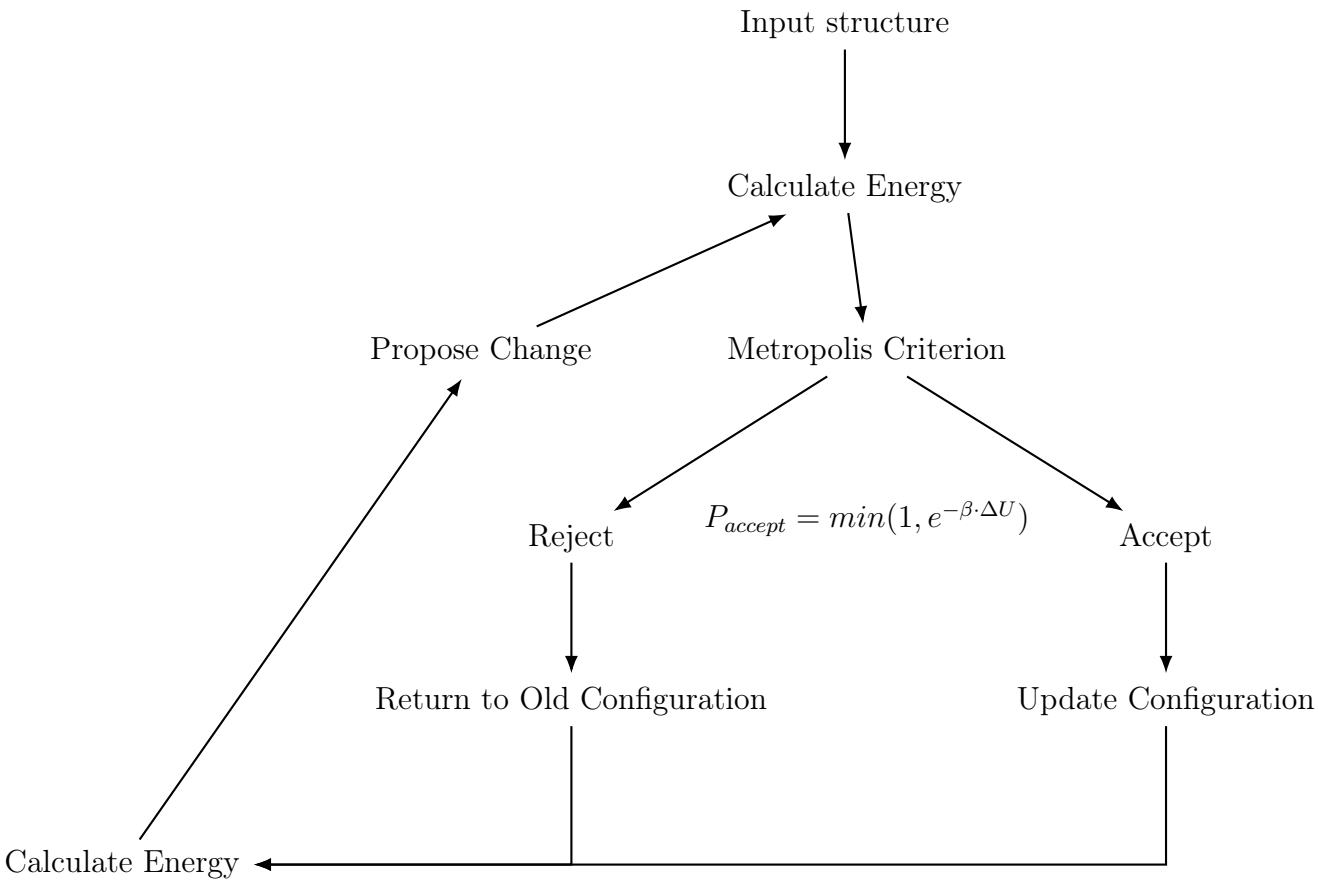

Figure 17: Scheme of Metropolis Monte Carlo algorithm.

2.2.2 Molecular Dynamics

Molecular dynamics is another very popular method for simulating chemical systems. This method treats chemical species as a classical many-body system. This can be done to systems, in which vibrational, rotational and other quantum effects can be effectively disregarded. As we discussed in the introduction to this chapter, this is a relevant ap-

proximation for systems of sufficient size. This method relies on forces acting on chemical species which are computed from potentials. The motion of particles is governed by Newton's equations of motion (EOM):

$$m_i \frac{d^2 \vec{r_i}(t)}{dt^2} = \vec{f_i}(t), \tag{10}$$

where m_i is the mass of particle i, $\vec{r_i}(t)$ its position at time t, and $\vec{f_i}(t)$ the force acting on it.

From these forces we then proceed to integration of Newton's second law of motion from time t to $t + \Delta t$. Δt represents time of one molecular dynamics step. This gives us the prediction of positions at time $t + \Delta t$. One of the most common integration methods used is Verlet method, mathematically written as :

$$\vec{r_i}(t + \Delta t) = 2\vec{r_i}(t) - \vec{r_i}(t - \Delta t) + \Delta t^2 \frac{\vec{f_i}(t)}{m_i}. \tag{11}$$

In the course of a simulation, a sequence of configurations is generated, commonly referred to as a trajectory. Provided that the simulation is sufficiently long and ergodic, time-averaged quantities computed along this trajectory converge to the corresponding ensemble averages. However in its pure form this method samples configurations in the microcanonical ensemble (NVE), where number of particles, volume and total energy are conserved. This is a rather hard limitation. Instead of fixed energy, it is much more favourable to have fixed temperature as a result of averaged energies. This is achieved by introducing a thermostat, which modifies the simulation of the system in such a way that the method effectively samples the canonical (NVT) ensemble , where the probability of a given state is weighted by the Boltzmann factor $\exp(-E/k_{\mathrm{B}}T)$. Most thermostats pair the simulated system to a thermal reservoir, which exists at fixed temperature and is able to exchange energy with the system. In this way the kinetic energy of the particles fluctuates around a target value corresponding to the chosen temperature. The reservoir itself is not simulated explicitly, but rather introduced mathematically by modifying the equations of motion. However, this approach can introduce ergodicity issues and small deviations arising from the numerical integrators.

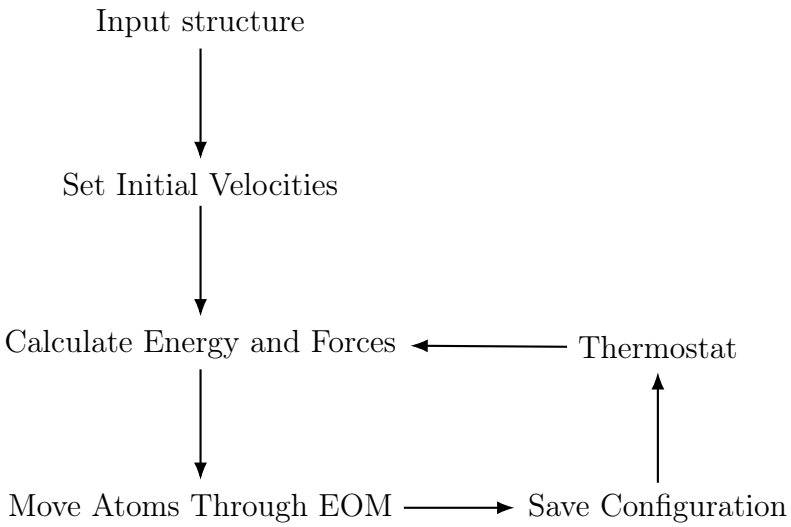

Figure 18: Scheme of molecular dynamics simulation.

2.2.3 Hamiltonian Monte Carlo

The method employed in our study is Hamiltonian Monte Carlo, which can be viewed as a hybrid between Metropolis Monte Carlo and molecular dynamics. The main distinction between classical Metropolis Monte Carlo and the method employed in our work, is that the proposal for a change in configuration will be generated by molecular dynamics integration of Newton's laws of motion. At the beginning of each proposal, the velocities drawn from the Maxwell-Boltzmann distribution will be randomly distributed among the beads and n_{steps} steps, with Δt time difference will be done. After this, the resulting configuration will be passed to Metropolis criterion and evaluated in the same way as described in previous sections. The main advantage of this approach is proposal generation which is in its core related to physical behaviour of the many-body system along with the fact, that even after using molecular dynamics, the Metropolis criterion still keeps our sampling in canonical ensemble without the explicit need to use a thermostat. The changes proposed are therefore usually more physically realistic due to the nature of molecular dynamics, yet still avoid the issues associated with thermostats. This ultimately leads to more efficient sampling.

2.3 Technical Details

We now address several technical considerations, which concern the difficulties of simulating concentrated and charged systems.

Computational time is a major limitation of computational simulations. Sampling in these systems is often very difficult, due to the complexity of the simulation. Direct pairwise calculation of Coulomb interactions among N particles scales with $\mathcal{O}(N^2)$, which is unfeasible for larger systems. Therefore we have to resort to more complex methods for calculation of these potentials. There exist many methods to perform fast and scalable calculations of Coulomb interaction[39,40]. For this study we have chosen P^{2}NFFT belonging to the family of mesh-FFT methods, which split Coulomb potential into short range part, calculated through classical summation, and long range part, which puts charges onto a mesh and then solves the Poisson equation using a fast Fourier transform. This algorithm scales as $\mathcal{O}(N \log N)$ which is a dramatic increase in speed.

However this alone provides insufficient acceleration to render the simulations practical on a single CPU. Therefore we have to employ high performance message passing interface and run calculations for our simulation on multiple CPUs. We are using ScaFaCoS[41] library implementation of Coulomb solvers. All of our simulations will be executed on 12 CPUs, until adequate sampling is acquired.

Sampling of the simulations is first evaluated qualitatively by monitoring the evolution of the radius of gyration, R_{g}, of several independent chains as a function of simulation cycles. A stable and fluctuating behaviour of R_{g} over time indicates that the system is properly sampling conformational space. Examples of these evolutions can be found in Appendix. To complement this visual inspection, we also perform a quantitative analysis of the correlation time of the data.

The correlation time, τ, is defined as

$$\tau = \sum_{k=1}^{\infty} c_k, \tag{12}$$

where c_k denotes the normalized autocorrelation function at lag k. Specifically,

$$c_k = \frac{\langle \Delta X_i, \Delta X_{i+k} \rangle}{\langle \Delta X^2 \rangle}, \tag{13}$$

with ΔX_i representing the deviation of an observable X_i from its mean value, approximated as $\Delta X_i \simeq X_i - \overline{X}$. In this formulation, c_k measures how strongly two data points

separated by k sampling steps are correlated. A rapid decay of c_k with increasing k corresponds to weak correlations and hence more efficient sampling, while slow decay indicates that configurations remain correlated over longer timescales.

Once the correlation time is determined, the data are divided into statistically independent blocks. Statistical properties, such as averages and error estimates, are then computed on the block-averaged data to ensure that the results reflect independent sampling[42].

2.4 Simulation Protocol

In order to perform the simulations, it is necessary to define the set of parameters that govern the interactions between beads and the dynamics of the sampling procedure. The parameters employed in our simulations are summarized as follows. Mass of all beads is equal to 50 atomic mass units. Bonded interactions are described by a harmonic potential characterized by an energy scale $\varepsilon_{\mathrm{b}} = 80\, k_{\mathrm{B}}T$ and an equilibrium bond length $r_0 = 0.3\,\mathrm{nm}$. Non-bonded interactions are modeled using a soft repulsive sphere (SRS) potential with energy scale $\varepsilon_{\mathrm{nb}} = 1\, k_{\mathrm{B}}T$ and cutoff distance $c = 2r_0$. For hydrophobic beads, this interaction is augmented by a soft attractive sphere (SAS) contribution, scaled by the dimensionless parameter θ, which controls the strength of the hydrophobic attraction. In particular, $\theta = 1.1$ corresponds to conditions of a poor solvent. Electrostatic interactions are included through the Coulomb potential expressed in terms of the Bjerrum length, with $l_{\mathrm{B}} = 0.7\,\mathrm{nm}$, corresponding to water-like screening at room temperature. Trial moves in Hamiltonian Monte Carlo are generated by short molecular dynamics trajectories with time step $\Delta t = 0.05$ simulation time units and number of steps $n_{\mathrm{steps}} = 100$, ensuring physically realistic proposals while retaining canonical ensemble sampling.

In total, we will investigate eight distinct core systems. The first distinction between these systems arises from the nature of one of the blocks. In all cases, one block is a polyelectrolyte, while the second block is either hydrophilic or hydrophobic, as determined by the interaction potentials described in the previous sections.

Next, we differentiate between strong and weak polyelectrolytes. Strong polyelectrolytes are modeled with static charges, whereas weak polyelectrolytes are treated with a dynamic charge distribution that can fluctuate during the simulation.

Finally, we consider two different chain lengths, with block sizes of either 25 beads per block or 50 beads per block. For brevity, we will refer to these systems as 25–25 and 50–50, respectively, in both the text and figures. There will be a total number of 10 000 polymer beads in all simulations. This means that for the simulations of 50-50 copolymer there will be total of 100 chains and 200 chains for 25-25 copolymer.

This hierarchical classification yields the eight systems studied in this work.

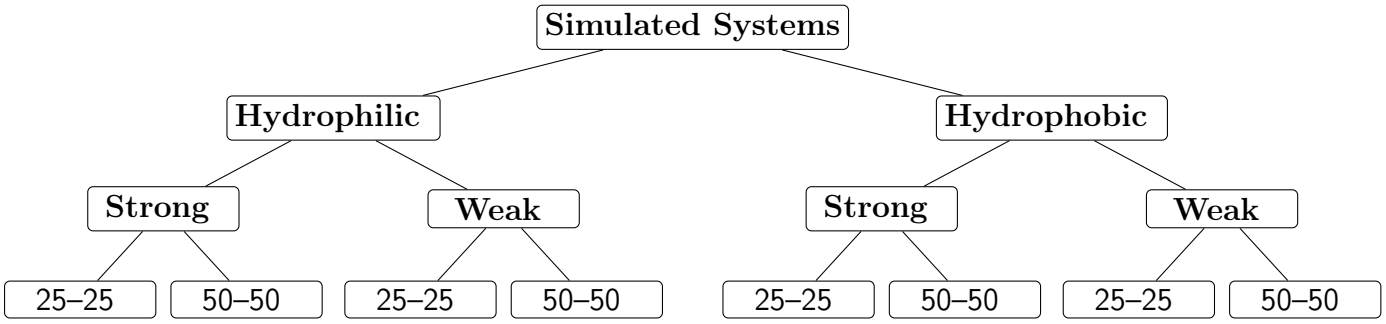

Figure 19: Division into 8 core simulated systems depicted graphically.

Furthermore, to study the effects of concentration of these systems, we will vary the size of PBC box in which the simulation takes place. These box sizes and corresponding monomer concentrations can be seen in Table 1. To also study effects of ionization, we

Table 1: Monomer concentration as a function of box size.

Box Size (nm)	**Monomer Concentration (M)**
15	4.920
20	2.076
25	1.063
30	0.615
35	0.387
40	0.260
60	0.0769
80	0.0324
100	0.0166
200	0.00208
400	0.000260

further divide the simulations into different degrees of ionizations. These are 0, 0.05, 0.10, 0.15, 0.20, 0.25 and 0.35.

In total we ran **616** simulations over multiple runs, until sufficient sampling was achieved. Expanded tree of one core system can be seen in Figure 20.

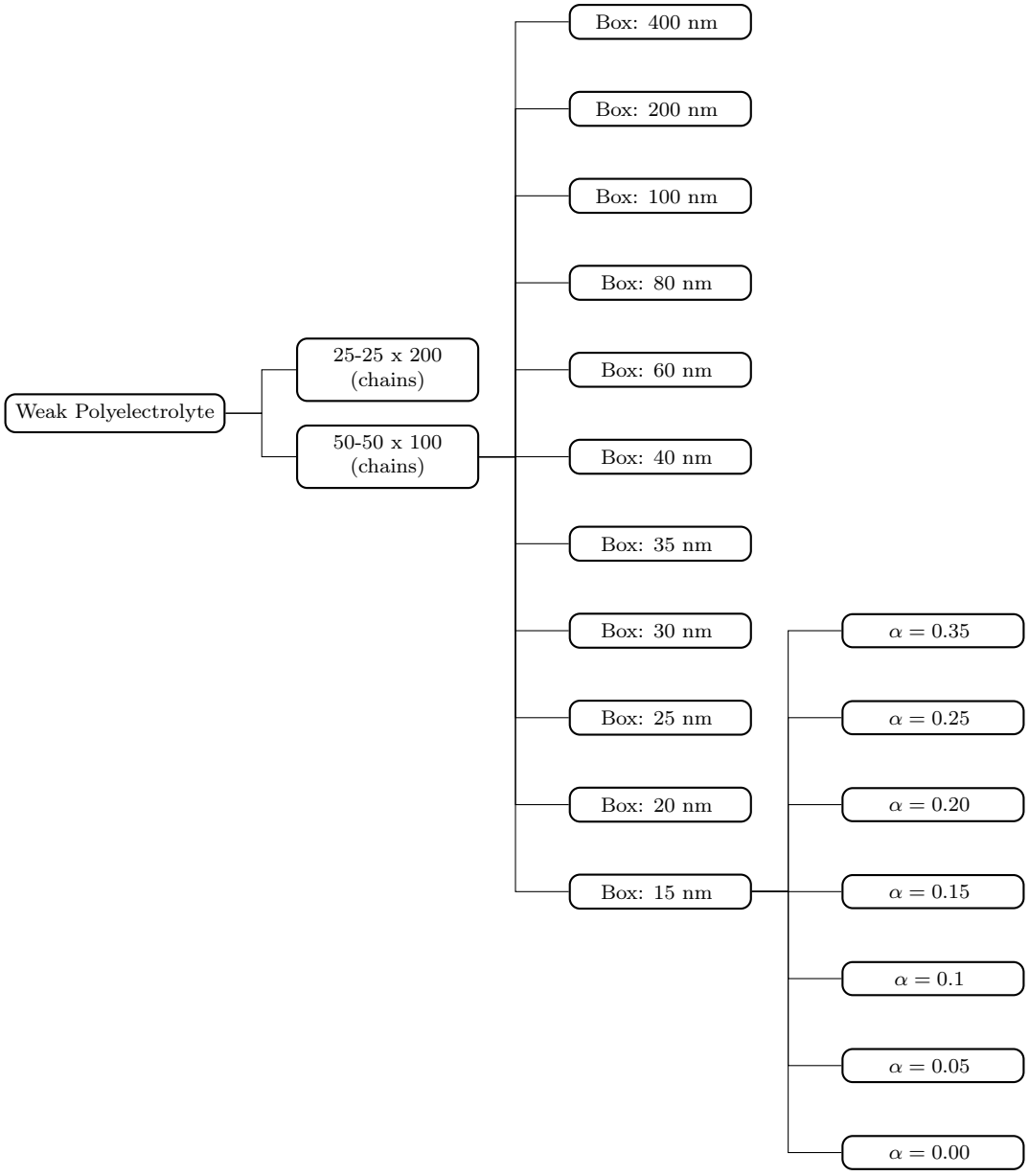

Figure 20: Structure of weak polyelectrolyte simulation configurations

3 Results and Analysis

Before presenting the results of our simulations, it is useful to first summarize several key findings that are well established in the literature.

Scaling of size for neutral polymers has been introduced in the introductory section and is extensively discussed in the literature[23,24,35,43]. In the dilute regime ($c < c^*$), polymer chains do not overlap, and their conformations remain unaffected by concentration. Consequently, the polymer size is independent of concentration,

$$R_g \propto c^0. \tag{14}$$

Once the concentration exceeds the overlap threshold ($c > c^*$), chains begin to interpenetrate. As a result, the polymer size exhibits a weak concentration dependence,

$$R_g \propto c^{-0.12}, \tag{15}$$

in agreement with scaling theory and simulation results[23,24].

Scaling of size for polyelectrolytes has likewise been reported in numerous studies[25,44–46]. In dilute solution ($c < c^*$), chains behave independently, and their size remains constant with concentration,

$$R_g \propto c^0. \tag{16}$$

Above the overlap concentration ($c > c^*$), however, electrostatic interactions are screened by overlapping chains, and the electrostatic blob model applies. In this regime, the chain size decreases with concentration according to

$$R_g \propto c^{-1/4}. \tag{17}$$

3.1 Doubly Hydrophilic Copolymers

For doubly hydrophilic copolymers, a combination of behaviors arising from both the polyelectrolyte and neutral polymer segments is expected. In the following sections, we first examine the influence of chain length and ionization, and subsequently address the

effects of concentration in the relevant systems.

3.1.1 Effects of Chain Length

We investigated the influence of chain length on the scaling behavior of polymer size. For clarity, all systems presented in this subsection correspond to the case of weak ionization. The effects of varying ionization strength will be addressed in a subsequent section. The dependence of R_g on concentration is shown in Figure 21 for 50–50 block copolymers and in Figure 22 for 25–25 block copolymers.

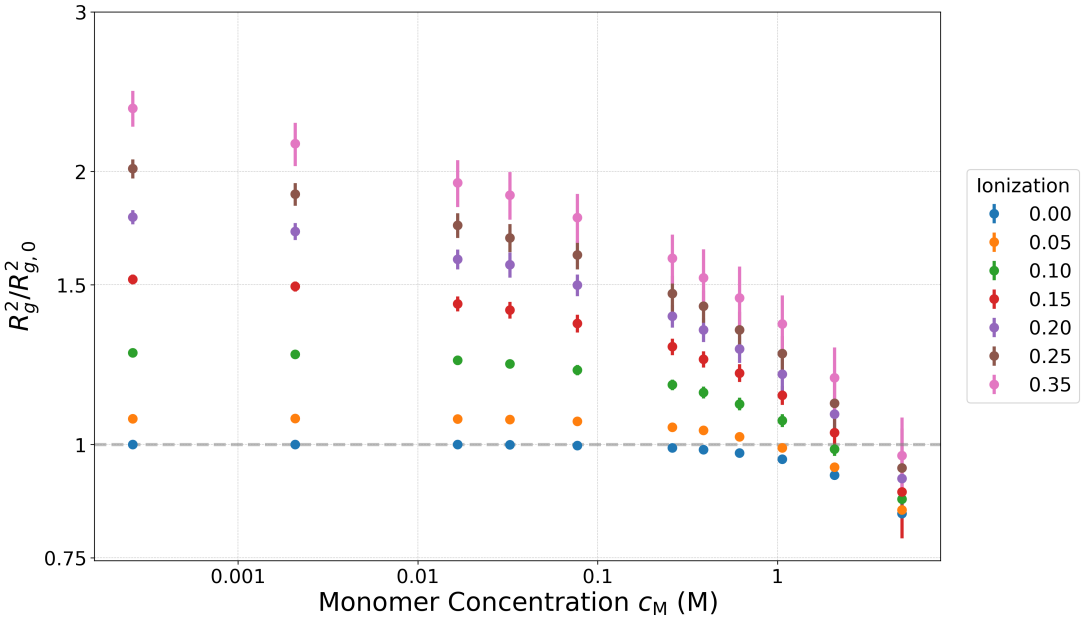

Figure 21: Normalized square of the radius of gyration, $R_g^2/R_{g,0}^2$, as a function of monomer concentration for a system of 100 symmetric 50–50 block copolymer chains at varying degrees of ionization. The normalization is taken with respect to the radius of gyration at the lowest ionization and lowest concentration. $R_{g,0}^2 = 6.1678\,\mathrm{nm}^2$ at $c_M = 0.00026\,\mathrm{M}$, Ionization $= 0$.

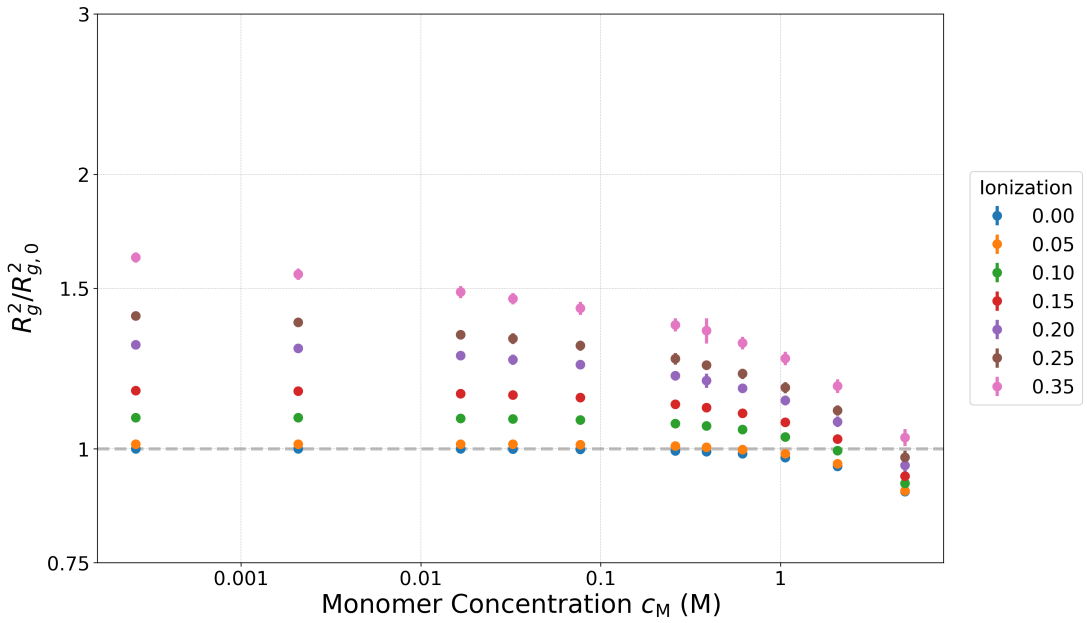

Figure 22: Normalized square of the radius of gyration, $R_g^2/R_{g,0}^2$, as a function of monomer concentration for a system of 200 symmetric 25-25 block copolymer chains at varying degrees of ionization. The normalization is taken with respect to the radius of gyration at the lowest ionization and lowest concentration. $R_{g,0}^2 = 2.5618\,\mathrm{nm}^2$ at $c_\mathrm{M} = 0.00026\,\mathrm{M}$, Ionization $= 0.$.

From these results, it can be observed that a reduction in chain length leads to an increase in the overlap concentration, c^*, at which the transition from the dilute to the semi-dilute regime occurs. At first glance, this trend can be attributed to a decrease in the correlation length that accompanies shorter chains. To examine this effect in greater detail, we decomposed the ratio $R_g^2/R_{g,0}^2$ into block-wise contributions, shown in Figure 23 for the 50-50 copolymer and in Figure 24 for the 25-25 copolymer.

In the case of the 50-50 system, scaling behavior characteristic of neutral polymers remains partially discernible, whereas in the 25-25 system this behavior is largely absent, with the reduction in size being dominated by contributions from the polyelectrolytic block. Our results are in good agreement with established theoretical and experimental literature on polymer solutions. Specifically, the scaling of overlap concentration with chain length differs markedly between neutral and polyelectrolytic systems: for neutral chains in good solvent[35], $c^* \sim N^{-4/5}$, while for salt-free polyelectrolytes[44], the much steeper dependence $c^* \sim N^{-2}$ is observed. This stronger scaling means that as the number of beads (or monomeric units) in the chain increases, the polyelectrolytic system reaches the overlap regime at significantly lower concentrations, i.e., it shows the onset

of chain–chain interactions "faster" with increasing chain length. This behavior aligns closely with prior reports, reinforcing that the electrostatic stretching of charged chains enhances excluded volume effects and shifts the overlap concentration downward more strongly than in neutral analogues. A direct comparison of the two systems is provided in Figure 25. Although indications of polyelectrolytic scaling can be detected for the 25-25 copolymer, the crossover into the semi-dilute regime appears to occur only at higher concentrations, beyond the range accessible in the present dataset. Consequently, for the purposes of this study, we focus our attention on the 50-50 copolymer system, as it more clearly exhibits the properties of interest.

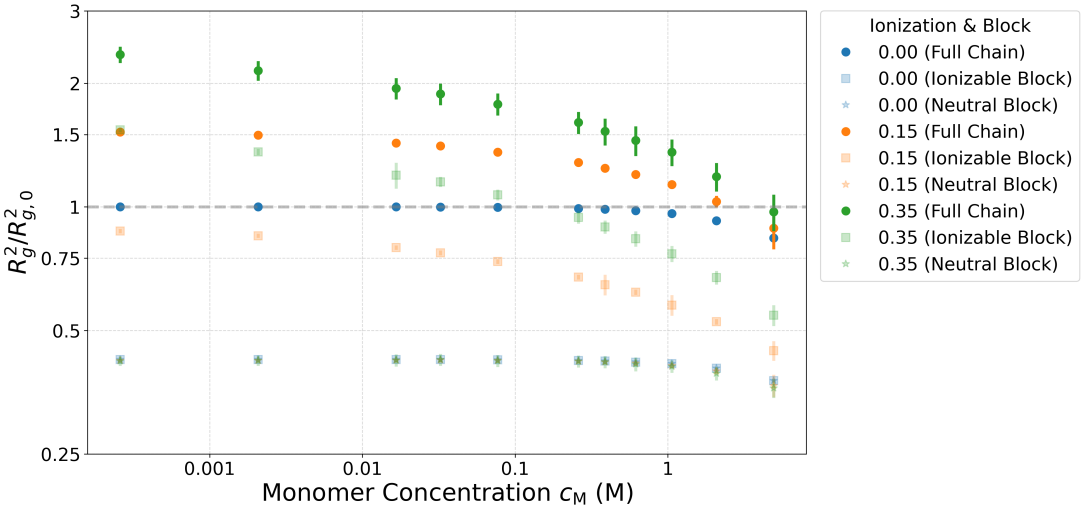

Figure 23: Normalized square of the radius of gyration, $R_g^2/R_{g,0}^2$, as a function of monomer concentration for a system of 100 symmetric 50–50 block copolymer chains at varying degrees of ionization. Split into contributing blocks. The normalization is taken with respect to the radius of gyration at the lowest ionization and lowest concentration. $R_{g,0}^2 = 6.1678\,\mathrm{nm}^2$ at $c_\mathrm{M} = 0.00026\,\mathrm{M}$, Ionization $= 0$.

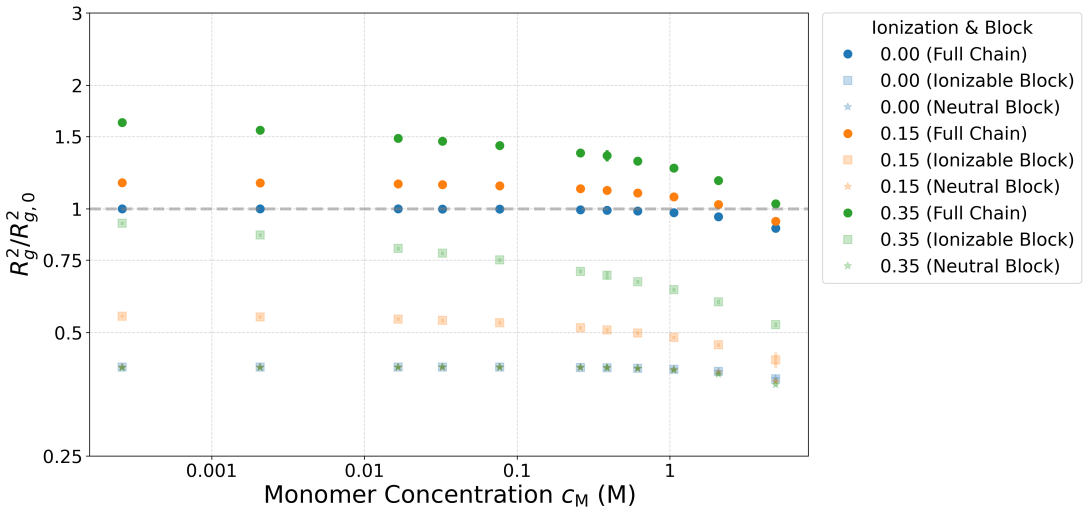

Figure 24: Normalized square of the radius of gyration, $R_g^2/R_{g,0}^2$, as a function of monomer concentration for a system of 200 symmetric 25-25 block copolymer chains at varying degrees of ionization. Split into contributing blocks. The normalization is taken with respect to the radius of gyration at the lowest ionization and lowest concentration. $R_{g,0}^2 = 2.5618\,\mathrm{nm}^2$ at $c_M = 0.00026\,\mathrm{M}$, Ionization $= 0$.

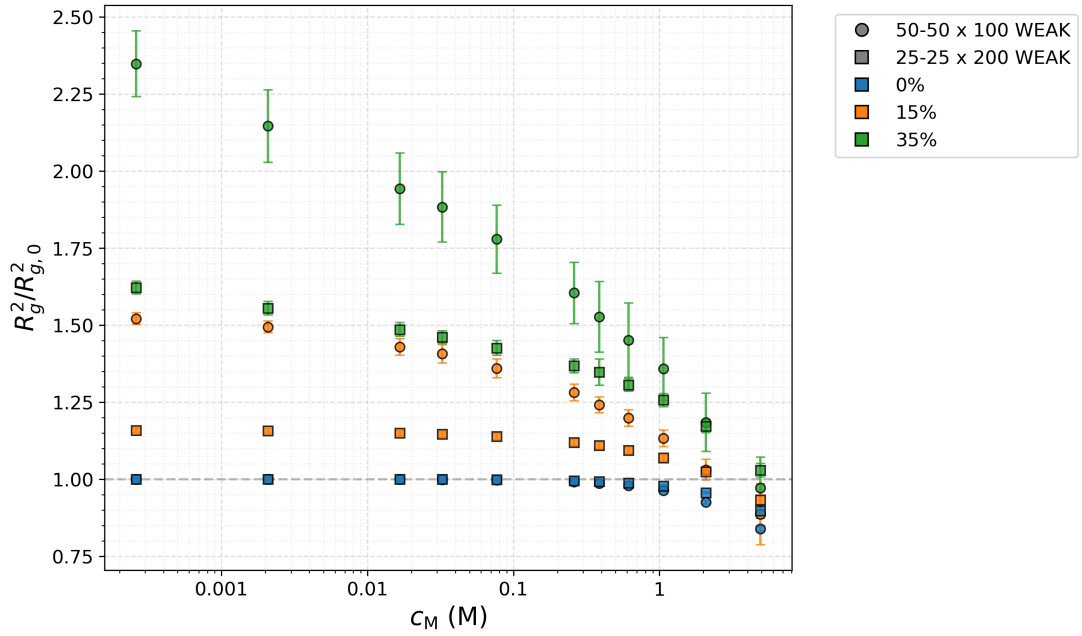

Figure 25: Normalized square of the radius of gyration, $R_g^2/R_{g,0}^2$, as a function of monomer concentration for both systems. Weak refers to the ionization type which will be discussed later. The normalization is taken with respect to the radius of gyration at the lowest ionization and lowest concentration. $R_{g,0}^2$ remains the same as in Figures 21 and 22.

3.1.2 Effects of Ionization

In this work, we investigated the effects of ionization by contrasting a weak polyelectrolyte model, in which charges are mobile, with a strong polyelectrolyte model, in which charges are fixed. A direct comparison of weak and strong ionization across both systems is provided in Figure 26.

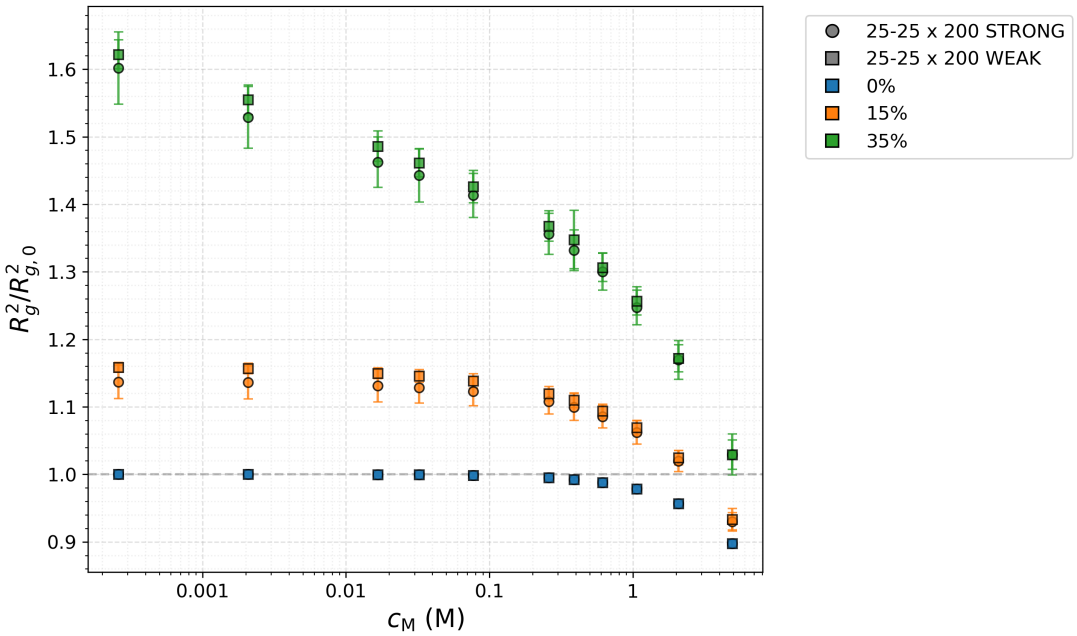

Figure 26: Normalized square of the radius of gyration, $R_g^2/R_{g,0}^2$, as a function of monomer concentration for both systems. Comparison of weak and strong ionization. The normalization is taken with respect to the radius of gyration at the lowest ionization and lowest concentration. $R_{g,0}^2(\text{strong}) = R_{g,0}^2(\text{weak}) = 2.5618\,\text{nm}^2$ at $c_M = 0.00026\,\text{M}$, Ionization $= 0$.

From this we conclude that, within the range of ionization fractions investigated, there is no discernible difference between our approximation of strong and weak polyelectrolytes. This implies that, under these conditions, the conformational response is governed primarily by the presence of charges rather than by the precise strength of ionization. This agrees well with scientific literature which shows, that at low degrees of ionization, the difference between weak and strong polyelectrolyte is negligible[47]. However, upon closer examination we found an interesting feature: Figure 27 presents the distributions of the squared radius of gyration, R_g^2, for the neutral block, the ionizable chain and neutral block under conditions of strong and weak ionization at both high and low concentrations. The panels correspond to different degrees of ionization, increasing from top to

bottom. Again, as we have seen in Figure 23, the increase in R_g^2 of the ionizable block is more pronounced at lower concentrations compared to systems at higher concentration. This behavior is expected, since in dilute conditions polymer chains are free to expand, whereas at higher concentrations chain–chain contacts suppress further growth in size. Repeatedly we have found that weak ionization leads to narrower distributions of the radius of gyration in the ionizable block. This indicates that charge mobility has indeed played a role in determining the final conformations. We expect that this mobility allowed the system to optimize the spatial arrangement of charges, which in turn led to a narrowing of the R_g distributions. These observations suggest that, although the mean value of R_g^2 remains largely unchanged, variations in the degree of ionization exert influence on the conformational statistics of the chains. In particular, the ionization strength governs the distributional width and shape of R_g^2, indicating that electrostatic interactions and charge mobility contribute to fine-tuning the equilibrium conformations beyond what is captured by the average R_g^2 measurement alone.

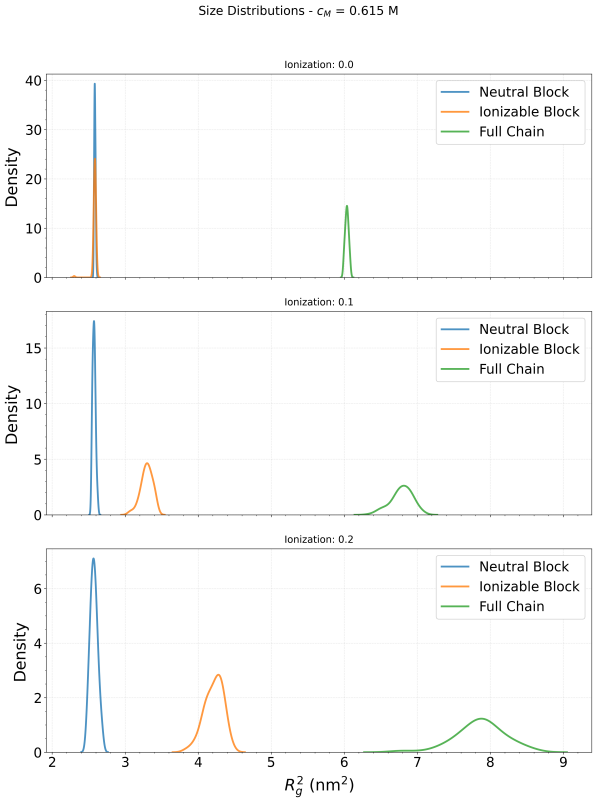

(a) Strong ionization at low concentration

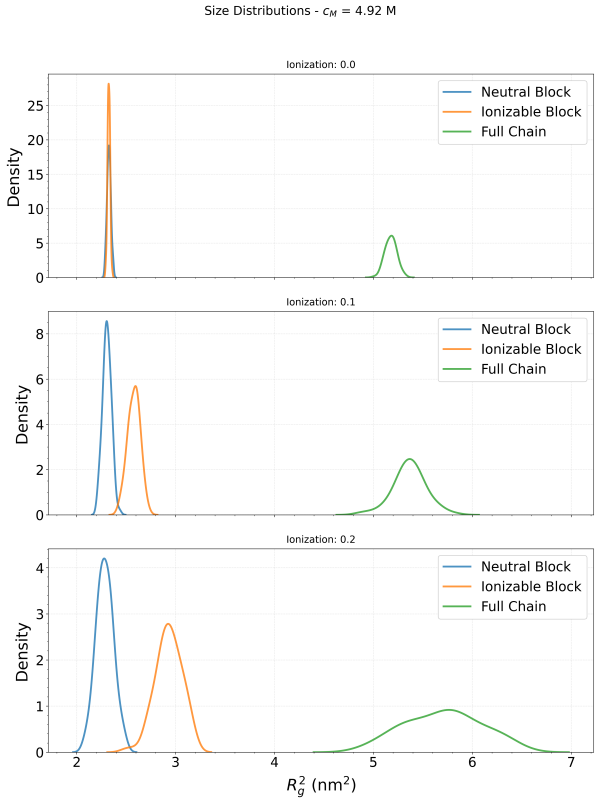

(b) Strong ionization at high concentration

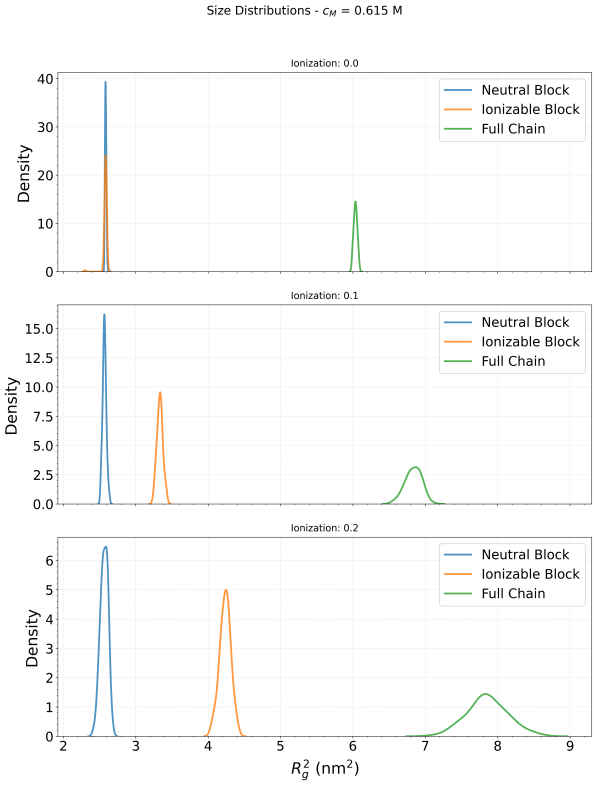

(c) Weak ionization at low concentration

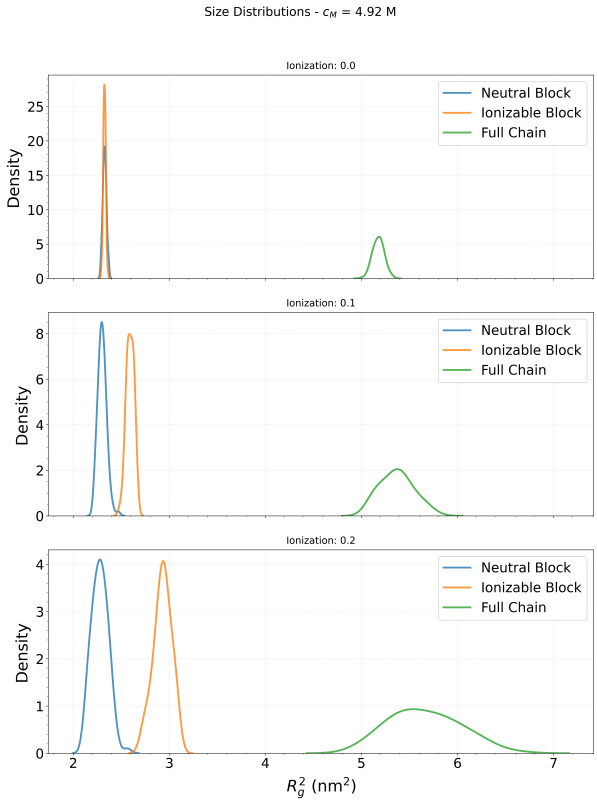

(d) Weak ionization at high concentration

Figure 27: Comparison of chain radius of gyration distributions at different concentrations and ionization strengths, showing that weak ionization leads to narrower distributions.

3.1.3 Effects of Concentration

To quantify the effects of concentration, we performed linear fits to our data and extracted the corresponding scaling exponents. These values were then compared to the theoretical predictions introduced earlier in this chapter notably Equations 15 and 17, allowing us to directly assess the extent to which our results agree with established scaling laws. Acquired results can be seen in Figure 28 and scaling exponents (slopes) of the semi-dilute regimes can be found in Table 2. The associated errors were smaller than the precision of the reported values and are therefore not explicitly listed.

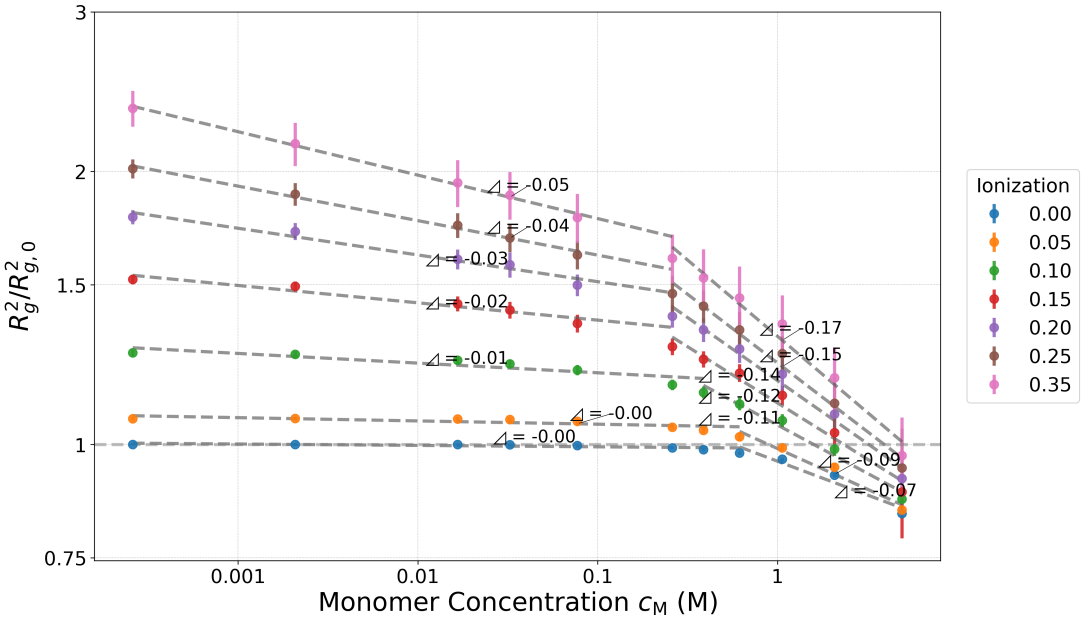

Figure 28: Normalized square of the radius of gyration, $R_g^2/R_{g,0}^2$, as a function of monomer concentration for a system of 100 symmetric 50–50 block copolymer chains at varying degrees of ionization with fitted exponents. The normalization is taken with respect to the radius of gyration at the lowest ionization and lowest concentration. $R_{g,0}^2$ remains the same as in Figure 21.

As shown in Figure 28, our results are in reasonable agreement with the theoretical expectations cited in Equations 15 and 17. In particular, we observe a crossover in scaling behavior upon entering the semi-dilute regime. With increasing ionization, the exponent governing the scaling of R_g with concentration gradually decreases. We anticipate that, over a broader concentration range, this exponent would asymptotically approach the theoretical value of $c^{-1/4}$ predicted for polyelectrolytes, or fall slightly short of it. Owing to the limited range of concentrations accessible in our study, the scaling behavior of neutral polymers could not be fully resolved. Nonetheless, when restricting the fit to

the two highest concentration points at zero ionization, we obtain an exponent of $c^{-0.12}$, consistent with the expected neutral polymer scaling. This confirms that our current concentration window is insufficient for a complete characterization of neutral polymer behaviour, but nevertheless captures aspects of both neutral and polyelectrolyte regimes. In addition, we have estimated the overlap concentration c^* at each ionization level. The overlap concentration c^* was estimated as the intersection point of the two linear fits corresponding to the dilute and semi-dilute regimes. As anticipated, the value of c^* decreases systematically with increasing degree of ionization, reflecting the enhanced chain expansion. These values are presented in Figure 29 and summarized in Table 3. Again estimated errors were smaller than the precision of the values and therefore were not explicitly listed.

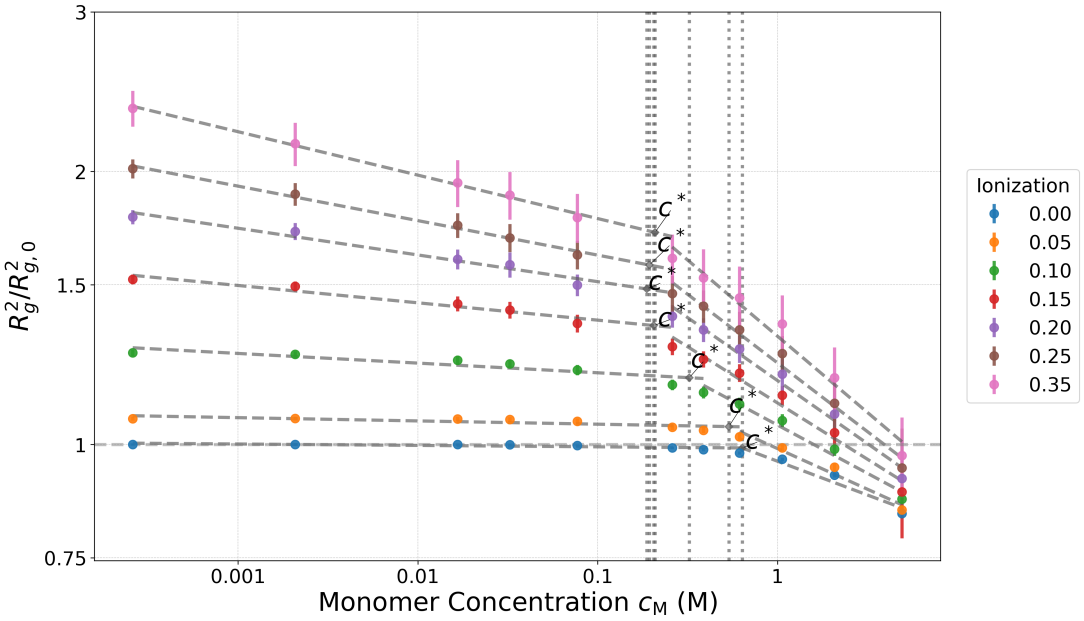

Figure 29: Normalized square of the radius of gyration, $R_g^2/R_{g,0}^2$, as a function of monomer concentration for a system of 100 symmetric 50–50 block copolymer chains at varying degrees of ionization with approximated overlap concentrations. The normalization is taken with respect to the radius of gyration at the lowest ionization and lowest concentration. $R_{g,0}^2$ remains the same as in Figure 21.

To provide a qualitative visualization of the conformational changes, we include in Figure 30 a series of representative simulation snapshots taken at increasing concentrations. These images serve as a visual guide to complement the quantitative analysis presented above.

Ionization	Slope
0.00	-0.07
0.05	-0.09
0.10	-0.11
0.15	-0.12
0.20	-0.14
0.25	-0.15
0.35	-0.17

Table 2: Semi-dilute regime slopes from $R_g^2/R_{g,0}^2$ vs. monomer concentration.

Ionization	$c^\star$ (M)
0.00	0.636
0.05	0.536
0.10	0.323
0.15	0.205
0.20	0.187
0.25	0.158
0.35	0.122

Table 3: Crossover concentrations $c^\star$ for different ionization fractions.

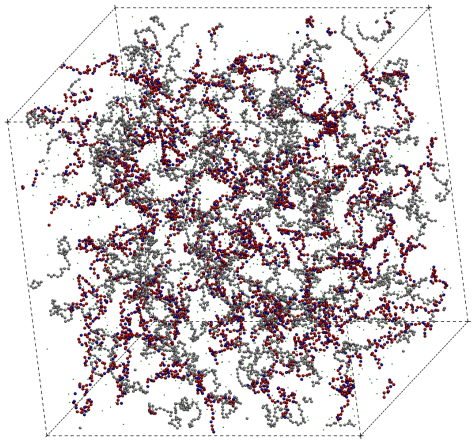

(a) $c_\mathrm{M} = 1.063$ M

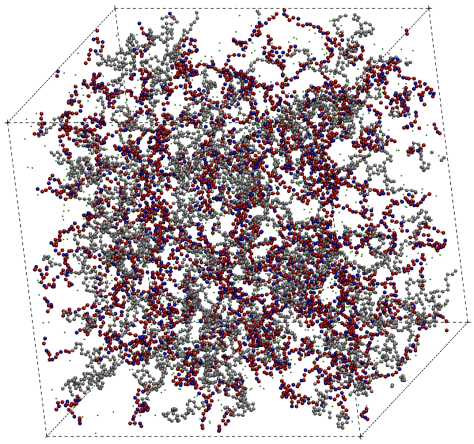

(b) $c_\mathrm{M} = 2.076$ M

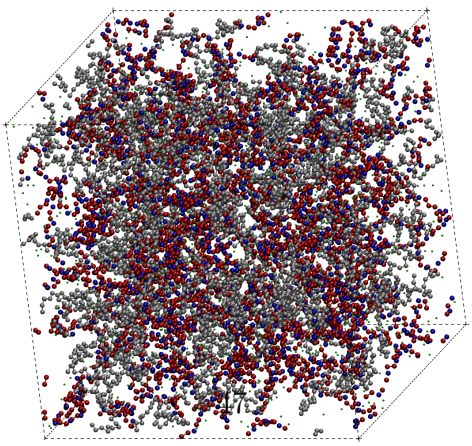

(c) $c_\mathrm{M} = 4.920$ M

3.2 Amphiphilic Copolymers

In amphiphilic copolymers, the hydrophobic block is expected to drive aggregation in solution. At sufficiently high concentrations, or above the critical micelle concentration, the hydrophobic segments cluster together to minimize unfavorable contacts with the solvent. We also note that the reliability of our results decreases at higher concentrations and higher degrees of ionization. In these regimes, the strong hydrophobic potentials significantly hinder efficient sampling in our Monte Carlo simulations, leading to increased statistical uncertainty. Consequently, the reported data exhibit larger errors under these conditions as seen in Figure 31. Nevertheless, the qualitative trends remain consistent with theoretical expectations, and we consider the results to capture the essential features of the system's behavior, even if some of the quantitative values should be interpreted with caution.

3.2.1 Effects of Chain Length

Similar to the case of the doubly hydrophilic systems, we find that the scaling behavior of the 25-25 block copolymer cannot be fully resolved within the concentration range accessible to our simulations. The results for this comparison are presented in Figure 31 for the 50-50 block system and in Figure 32 for the 25-25 block system. In both cases, the observed limitations primarily arise from the block that carries no charge, which suppresses the development of clear scaling behavior within the studied range. As a consequence, we restrict our discussion in what follows to the 50-50 block copolymer.

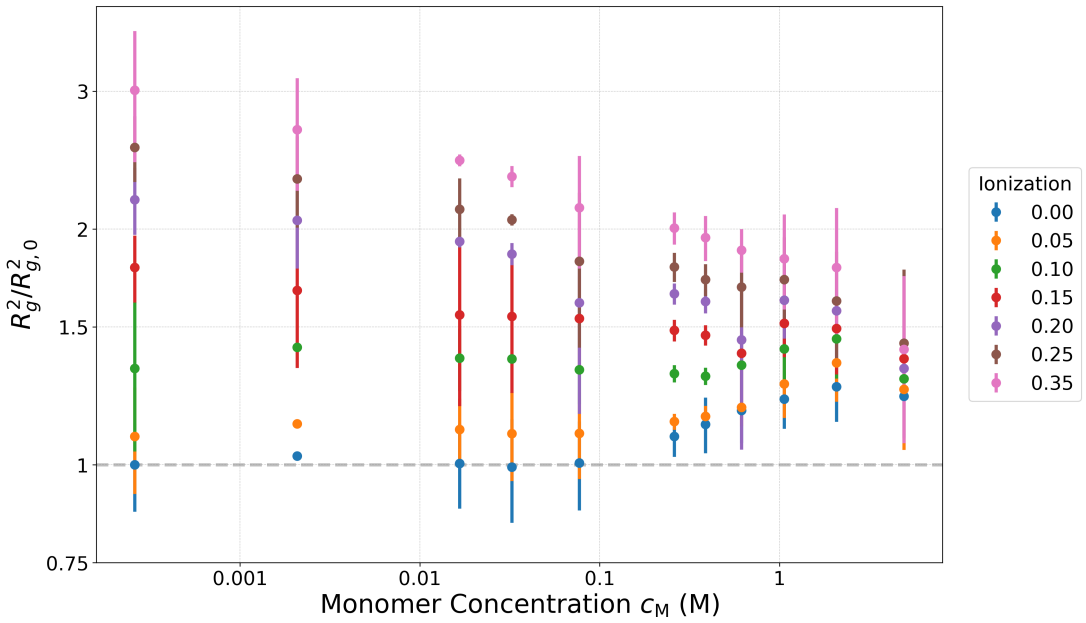

Figure 31: Normalized square of the radius of gyration, $R_g^2/R_{g,0}^2$, as a function of monomer concentration for a system of 100 symmetric 50–50 block amphiphilic copolymer chains at varying degrees of ionization. The normalization is taken with respect to the radius of gyration at the lowest ionization and lowest concentration. $R_{g,0}^2 = 4.1061\,\mathrm{nm}^2$ at $c_\mathrm{M} = 0.00026\,\mathrm{M}$, Ionization $= 0$.

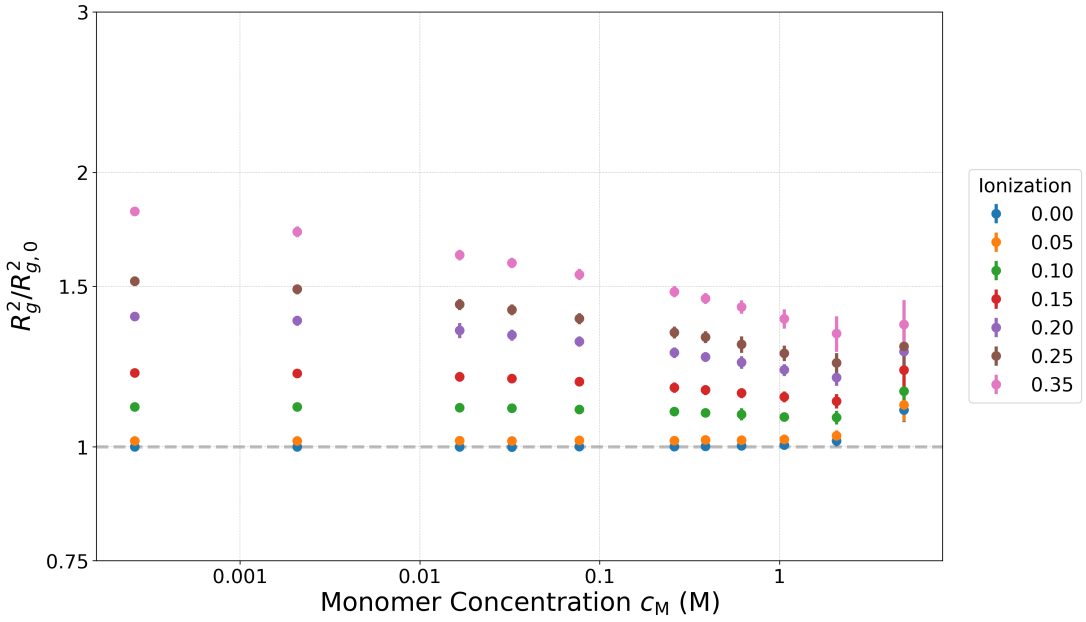

Figure 32: Normalized square of the radius of gyration, $R_g^2/R_{g,0}^2$, as a function of monomer concentration for a system of 200 symmetric 25-25 block amphiphilic copolymer chains at varying degrees of ionization. The normalization is taken with respect to the radius of gyration at the lowest ionization and lowest concentration. $R_{g,0}^2 = 1.9597\,\mathrm{nm}^2$ at $c_\mathrm{M} = 0.00026\,\mathrm{M}$, Ionization $= 0$.

3.2.2 Effects of Ionization

As observed previously for the doubly hydrophilic system, the distinction between strong and weak ionization likewise does not exert a significant influence on the overall size of the polymer in the amphiphilic case. This trend is illustrated in Figure 33.

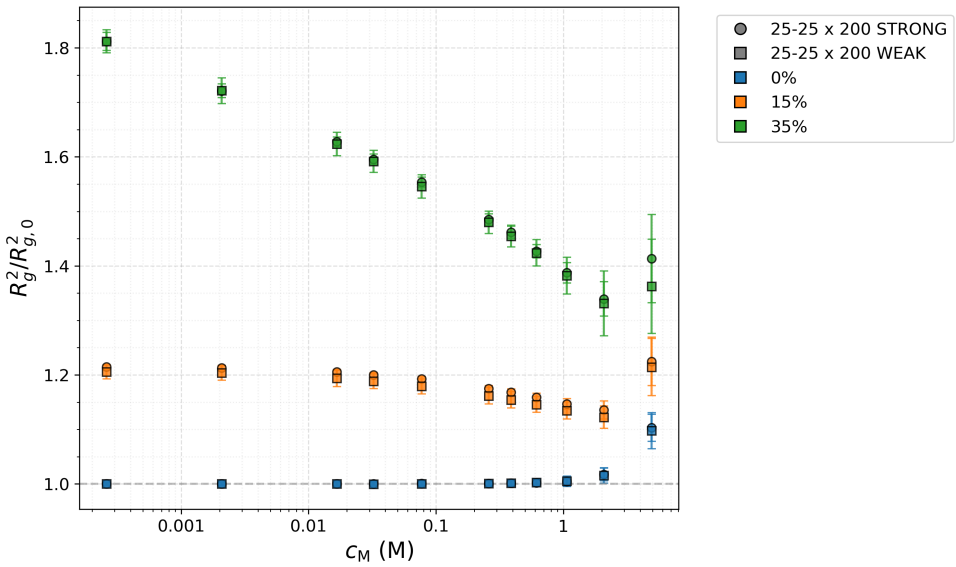

Figure 33: Normalized square of the radius of gyration, $R_g^2/R_{g,0}^2$, as a function of monomer concentration for both systems. Comparison of weak and strong ionization for amphiphilic copolymer. The normalization is taken with respect to the radius of gyration at the lowest ionization and lowest concentration. $R_{g,0}^2(\text{strong}) = R_{g,0}^2(\text{weak}) = 1.9597\,\text{nm}^2$ at $c_\text{M} = 0.00026\,\text{M}$, Ionization $= 0$.

3.2.3 Effects of Concentration

The effects of concentration represent an especially interesting aspect of the behavior of amphiphilic copolymers. With increasing concentration, we observed the formation of aggregates, consistent with the expected clustering of the hydrophobic segments. Interestingly, this aggregation is accompanied by an overall increase in the square radius of gyration, R_g^2, as shown in Figure 31. This result may at first appear counterintuitive, since aggregation is typically associated with compaction of individual chains. However, closer inspection reveals that the observed increase in R_g^2 can be traced primarily to the contribution of the hydrophobic block as seen in Figure 34. As the hydrophobic domains cluster, the hydrophobic segments are stretched around the aggregate core in order to shield it from solvent exposure. This enables multiple new way in which beads can surround themselves with other hydrophobic beads without the decrease in R_g^2. This stretching increases

their effective contribution to the overall radius of gyration and, consequently, elevates the total R_g^2 of the chain.

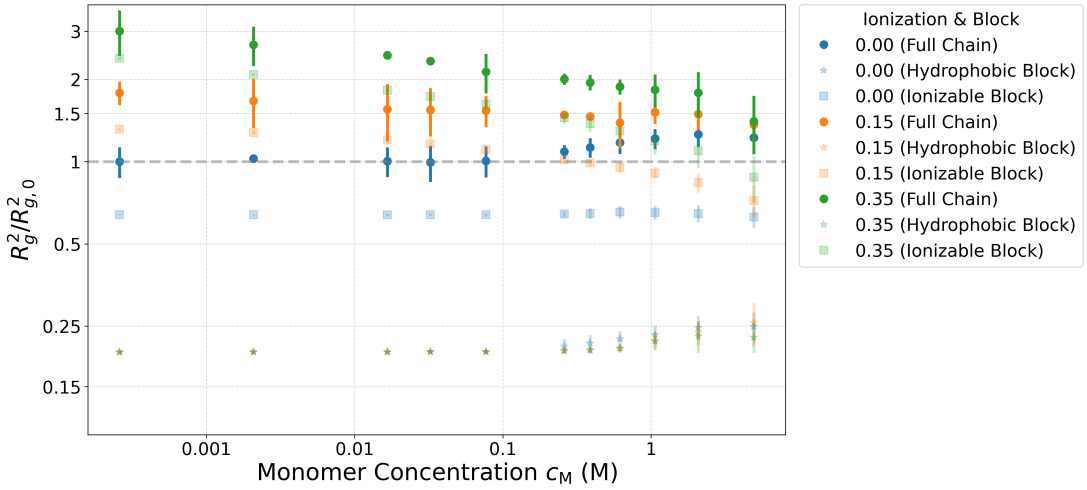

Figure 34: Normalized square of the radius of gyration, $R_g^2/R_{g,0}^2$, as a function of monomer concentration for a system of 100 symmetric 50–50 block copolymer chains at varying degrees of ionization. Split into contributing blocks. The normalization is taken with respect to the radius of gyration at the lowest ionization and lowest concentration.$R_{g,0}^2$ remains the same as in Figure 31.

Furthermore, the decrease in R_g^2 observed at the highest concentration is attributed to the scaling behavior of the polyelectrolyte block, which begins to dominate over the contribution from the hydrophobic block. In this regime, the conformational statistics of the charged block follow the expected semidilute polyelectrolyte scaling, leading to a reduction of the overall R_g^2. This transition highlights the competition between hydrophobic aggregation at intermediate concentrations and polyelectrolyte scaling at high concentrations. Representative snapshots of these systems are shown in Figure 35, providing a qualitative visualization of this behavior.

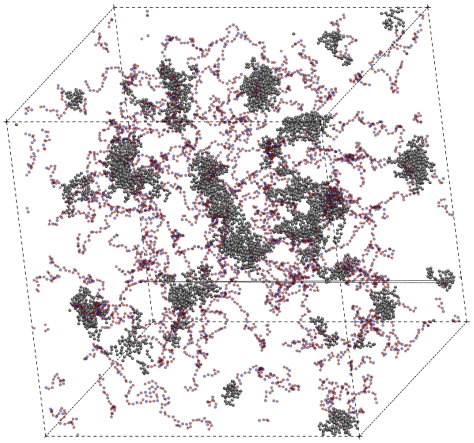

(a) $c_{\mathrm{M}} = 1.063$ M

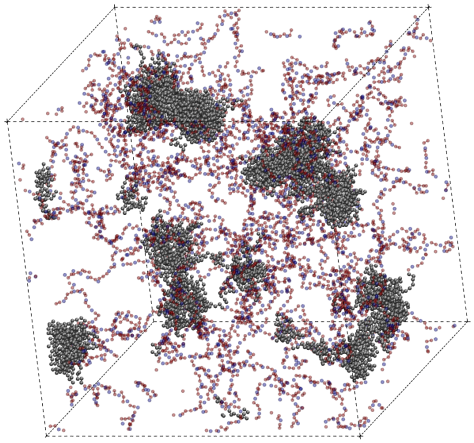

(b) $c_{\mathrm{M}} = 2.076$ M

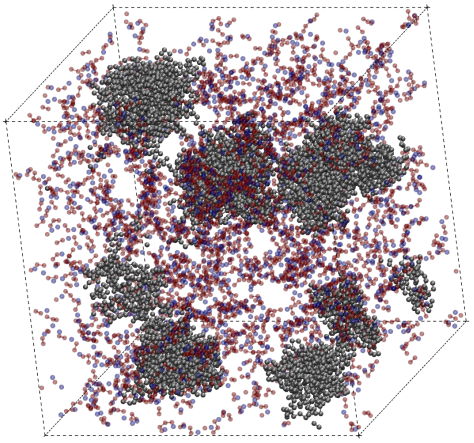

(c) $c_{\mathrm{M}} = 4.920$ M

Figure 35: Snapshots of amphiphilic block copolymer systems, with increasing concentrations.

4 Future perspectives

We have studied two types of block copolymer systems. While the results obtained are promising, it is important to acknowledge potential limitations, unexplored directions, and opportunities for future work.

One natural extension would be to employ more sophisticated interaction potentials based on real monomers. Although our focus here has been on the most general case, we expect that potentials derived from all-atom simulations could yield new and important insights, especially for systems where specific interactions play a dominant role and cannot be captured by generic repulsive–attractive models. A commonly used pipeline for this purpose is the construction of coarse-grained potentials from all-atom statistics, followed by refinement through iterative Boltzmann inversion[48]. While such an approach introduces additional complexity and computational cost—particularly at high concentrations—it remains a fascinating direction for future studies.

Another avenue would be to explore systems at higher degrees of ionization. In this work, we limited our investigation to ionization levels up to 0.35, mainly to balance computational cost with the breadth of data collected. This was not due to a lack of expected phenomena; on the contrary, we anticipate that at higher ionization the interplay between polyelectrolytic and neutral blocks could reveal even richer behavior.

Closely related to the question of ionization is the role of added salt. Since counterions and screening strongly influence the behavior of charged block copolymers, it would be highly beneficial to extend this work toward varying salt concentrations. Furthermore, valency of the added salt is also of vital importance and we suspect detailed study would yield interesting results.

A further direction would be to investigate block copolymers with unequal block lengths. In the present work, we focused on symmetric systems with equal block fractions in order to isolate general trends and avoid complications arising from compositional asymmetry. However, varying the block ratio is known to have a profound effect on phase behavior, aggregation, and self-assembly pathways. For example, asymmetric diblocks often exhibit shifts in critical micelle concentrations, domain spacings, and preferred morphologies compared to their symmetric counterparts. Extending the current study to

include such variations would therefore provide a more comprehensive picture of the interplay between block architecture and emergent mesoscale structures.

Finally, in the case of amphiphilic block copolymers, it would be valuable to examine a wider range of the attractive potential parameter, θ. Ideally, one could map aggregation concentrations across different values of θ. Although such a detailed study lies beyond the broad, general scope of the present work, it represents an exciting challenge for future research.

5 Conclusion

In this thesis, we studied concentrated systems of two different block copolymers using a coarse-grained chain model in implicit solvent (water) and the Hamiltonian Monte Carlo method. Our analysis focused on the effects of chain length, ionization, and concentration.

In both copolymer systems, we found that longer chains exhibit lower overlap and interaction concentrations, consistent with more polymer-like scaling behaviour. At the low degrees of ionization examined, no significant differences were observed between strongly and weakly ionized cases. However, systems with weak ionization displayed a narrower distribution of the radius of gyration, which we attribute to optimization of charge positions along the chains.

For doubly hydrophilic block copolymers, the scaling behaviour reflected an effective mixture of polyelectrolyte-like and neutral polymer characteristics. This mixture was biased toward polyelectrolytic scaling, as the neutral block contribution became significant only at higher concentrations.

In amphiphilic block copolymers, we observed aggregation at high concentrations, leading to an increase in R_g as chains wrapped around hydrophobic cores. At the highest concentrations, however, R_g decreased, which we attribute to the stronger scaling of the polyelectrolytic block relative to the hydrophobic block.

Overall, these findings clarify how chain length, ionization, and concentration interplay to determine conformational and aggregation behaviour in concentrated block copolymer systems.

References

[1] Young, R. J.; Lovell, P. A. *Introduction to Polymers*; CRC Press, 2011.

[2] Sperling, L. H. *Introduction to Physical Polymer Science*; Wiley, 2005.

[3] Canevarolo, J., Sebastião V. *Polymer Science*; Carl Hanser Verlag, 2019.

[4] Dobrynin, A. V. Theory and simulations of charged polymers: From solution properties to polymeric nanomaterials. *Current Opinion in Colloid Interface Science* **2008**, *13*, 376–388.

[5] Li, L.; Xue, C.; Chang, Q.; Ren, X.; Li, N.; Yang, J.; Hu, S.; Xu, H. Polyelectrolyte Hydrogel-Functionalized Photothermal Sponge Enables Simultaneously Continuous Solar Desalination and Electricity Generation Without Salt Accumulation. *Advanced Materials* **2024**, *36*.

[6] Dogaris, I.; Pylypchuk, I.; Henriksson, G.; Abbadessa, A. Polyelectrolyte complexes based on a novel and sustainable hemicellulose-rich lignosulphonate for drug delivery applications. *Drug Delivery and Translational Research* **2024**, *14*, 3452–3466.

[7] Liu, Y.-C.; Chen, S.-H.; Kuan, C.-H.; Chen, S.-H.; Huang, W.-Y.; Chen, H.-X.; Wang, T.-W. Assembly of Interfacial Polyelectrolyte Complexation Fibers with Mineralization Gradient for Physiologically-Inspired Ligament Regeneration. *Advanced Materials* **2024**, *36*.

[8] Duan, J.; Fan, W.; Xu, Z.; Cui, L.; Wang, Z.; Nie, Z.; Sui, K. Polyelectrolyte-Mediated Modulation of Spatial Internal Stresses of Hydrogels for Complex 3D Actuators. *Angewandte Chemie International Edition* **2024**, *63*.

[9] Leibler, L. Theory of Microphase Separation in Block Copolymers. *Macromolecules* **1980**, *13*, 1602–1617.

[10] Mai, Y.; Eisenberg, A. Self-assembly of block copolymers. *Chemical Society Reviews* **2012**, *41*, 5969.

[11] Li, G.; Song, S.; Guo, L.; Ma, S. Selfassembly of thermo and pHresponsive poly(acrylic acid)*b*poly(*N*isopropylacrylamide) micelles for drug delivery. *Journal of Polymer Science Part A: Polymer Chemistry* **2008**, *46*, 5028–5035.

[12] Ramasamy, T.; Poudel, B. K.; Ruttala, H.; Choi, J. Y.; Hieu, T. D.; Umadevi, K.; Youn, Y. S.; Choi, H.-G.; Yong, C. S.; Kim, J. O. Cationic drug-based self-assembled polyelectrolyte complex micelles: Physicochemical, pharmacokinetic, and anticancer activity analysis. *Colloids and Surfaces B: Biointerfaces* **2016**, *146*, 152–160.

[13] Luo, Y.; Yao, X.; Yuan, J.; Ding, T.; Gao, Q. Preparation and drug controlled-release of polyion complex micelles as drug delivery systems. *Colloids and Surfaces B: Biointerfaces* **2009**, *68*, 218–224.

[14] Zhang, P.; Zhong, X.; Chai, Y.; Liu, Y. The effect of PVP-b-PMAA block copolymer on morphologies control of calcium carbonate. *Colloid and Polymer Science* **2008**, *286*, 1135–1141.

[15] Zhang, J.-P.; Cheng, S.-Z.; Li, X.-F.; Dong, J.-F. pH- and Temperature-Induced Micellization of the Dual Hydrophilic Block Copolymer Poly(methacrylate acid)-*b*-poly(*N*-(2-methacryloylxyethyl) pyrrolidone) in Aqueous Solution. *Acta Physico-Chimica Sinica* **2016**, *32*, 2018–2026.

[16] Nabiyan, A.; Max, J. B.; Schacher, F. H. Double hydrophilic copolymers – synthetic approaches, architectural variety, and current application fields. *Chemical Society Reviews* **2022**, *51*, 995–1044.

[17] Gineste, S.; Mingotaud, C. Double-hydrophilic block copolymer–metal ion associations: Structures, properties and applications. *Advances in Colloid and Interface Science* **2023**, *311*.

[18] Guo, L.; Wang, Y.; Steinhart, M. Porous block copolymer separation membranes for 21st century sanitation and hygiene. *Chemical Society Reviews* **2021**, *50*, 6333–6348.

[19] Samaddar, P.; Deep, A.; Kim, K.-H. An engineering insight into block copolymer self-assembly: Contemporary application from biomedical research to nanotechnology. *Chemical Engineering Journal* **2018**, *342*, 71–89.

[20] Bodratti, A. M.; Alexandridis, P. Amphiphilic block copolymers in drug delivery: advances in formulation structure and performance. *Expert Opinion on Drug Delivery* **2018**, *15*, 1085–1104.

[21] Nardin, C.; Widmer, J.; Winterhalter, M.; Meier, W. Amphiphilic block copolymer nanocontainers as bioreactors. *The European Physical Journal E* **2001**, *4*, 403–410.

[22] Sun, B.; Wang, P.; Shao, C.; Jiang, P.; Guo, Y.; Yan, S.; Fang, W. Amphiphilic comb-block copolymers synthesized by photoinitiated polymerization for stabilization of oil–water emulsion by solution self-assembly. *Fuel* **2025**, *385*, 134164.

[23] Rubinstein, M.; Colby, R. H. *Polymer Physics*; Oxford University Press, 2003.

[24] de Gennes, P.-G. *Scaling Concepts in Polymer Physics*; Cornell University Press, 1979.

[25] Dobrynin, A. V.; Colby, R. H.; Rubinstein, M. Scaling Theory of Polyelectrolyte Solutions. *Macromolecules* **1995**, *28*, 1859–1871.

[26] International Union of Pure and Applied Chemistry (IUPAC) Radius of Gyration. 2025; `https://doi.org/10.1351/goldbook.R05121`, IUPAC Compendium of Chemical Terminology, 5th edition (Gold Book).

[27] Metropolis, N.; Rosenbluth, A. W.; Rosenbluth, M. N.; Teller, A. H.; Teller, E. Equation of State Calculations by Fast Computing Machines. *The Journal of Chemical Physics* **1953**, *21*, 1087–1092.

[28] Labatut, B. *The MANIAC*; Penguin Group, 2024.

[29] Rajaraman, V. Frontier — World's First ExaFLOPS Supercomputer. *Resonance* **2023**, *28*, 567–576.

[30] Shi, R.; Qian, H.; Lu, Z. Coarsegrained molecular dynamics simulation of polymers:

Structures and dynamics. *WIREs Computational Molecular Science* **2023**, *13*.

[31] Kmiecik, S.; Gront, D.; Kolinski, M.; Wieteska, L.; Dawid, A. E.; Kolinski, A. Coarse-Grained Protein Models and Their Applications. *Chemical Reviews* **2016**, *116*, 7898–7936.

[32] Lavagnini, E.; Cook, J. L.; Warren, P. B.; Hunter, C. A. Translation of Chemical Structure into Dissipative Particle Dynamics Parameters for Simulation of Surfactant Self-Assembly. *The Journal of Physical Chemistry B* **2021**, *125*, 3942–3952.

[33] Miwatani, R.; Takahashi, K. Z.; Arai, N. Performance of Coarse Graining in Estimating Polymer Properties: Comparison with the Atomistic Model. *Polymers* **2020**, *12*, 382.

[34] Hsiao, P.-Y. Investigating the kinetics of single-chain expansion upon release in theta conditions. *Scientific Reports* **2025**, *15*.

[35] Teraoka, I. *Polymer Solutions*; Wiley-Interscience, 2002.

[36] Israelachvili, J. N. *Intermolecular and Surface Forces*, 3rd ed.; Academic Press, 2011.

[37] Milo, R.; Jorgensen, P.; Moran, U.; Weber, G.; Springer, M. BioNumbers—the database of key numbers in molecular and cell biology. *Nucleic Acids Research* **2010**, *38*, D750–D753.

[38] Frenkel, D.; Smit, B.; Ratner, M. A. *Understanding Molecular Simulation: From Algorithms to Applications*; AIP Publishing, 1997; Vol. 50.

[39] Cisneros, G. A.; Karttunen, M.; Ren, P.; Sagui, C. Classical Electrostatics for Biomolecular Simulations. *Chemical Reviews* **2013**, *114*, 779–814.

[40] GROMACS Development Team GROMACS User Manual version 2025. GROMACS, 2025; Accessed: 2025-08-16.

[41] Bolten, M.; Fahrenberger, F.; Halver, R.; Heber, F.; Hofmann, M.; Kabadshow, I.; Lenz, O.; Pippig, M.; Sutmann, G. ScaFaCoS, C subroutine library. `http://scafacos.github.com/`, `http://scafacos.github.com`.

[42] Janke, W. *Quantum Simulations of Complex Many-Body Systems: From Theory to Algorithms*; NIC Series; John von Neumann Institute for Computing, 2002; Vol. 10; pp 423–445.

[43] Young, C. D.; Marvin, M.; Sing, C. E. Conformationally averaged iterative Brownian dynamics simulations of semidilute polymer solutions. *The Journal of Chemical Physics* **2018**, *149*.

[44] G. Lopez, C.; Matsumoto, A.; Shen, A. Q. Dilute polyelectrolyte solutions: recent progress and open questions. *Soft Matter* **2024**, *20*, 2635–2687.

[45] Lopez, C. G.; Richtering, W. Conformation and dynamics of flexible polyelectrolytes in semidilute salt-free solutions. *The Journal of Chemical Physics* **2018**, *148*.

[46] Dobrynin, A.; Rubinstein, M. Theory of polyelectrolytes in solutions and at surfaces.

Progress in Polymer Science **2005**, *30*, 1049–1118.

[47] Castelnovo, M.; Sens, P.; Joanny, J. Charge Distribution on Annealed Polyelectrolytes. *arXiv preprint arXiv:cond-mat/9903345v1* **1999**, Submitted 23 March 1999, Condensed Matter – Soft Condensed Matter.

[48] Reith, D.; Pütz, M.; MüllerPlathe, F. Deriving effective mesoscale potentials from atomistic simulations. *Journal of Computational Chemistry* **2003**, *24*, 1624–1636.

Attachments

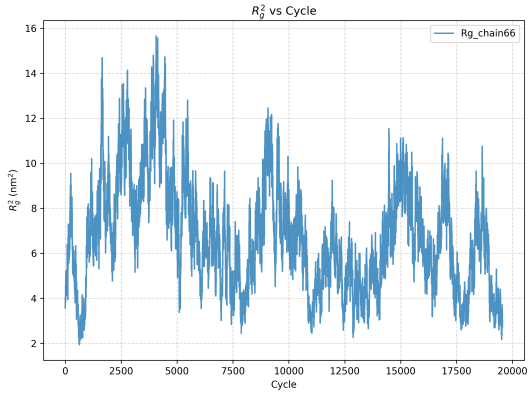

Poor sampling: the distribution is not well explored.

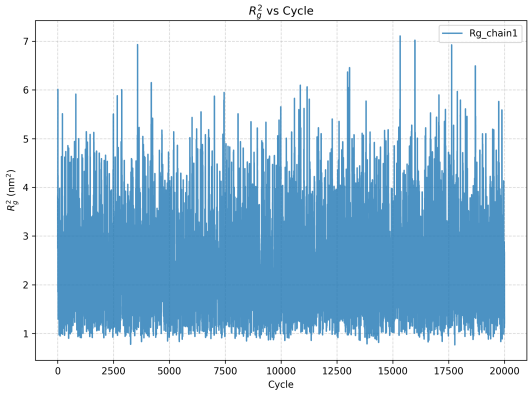

Good sampling: the distribution is thoroughly explored.

Comparison of sampling quality: (left) poor vs. (right) good sampling.